

1 **Identification of an endocannabinoid gut-brain vagal mechanism controlling**
2 **food reward and energy homeostasis**

3
4
5 Chloé Berland¹, Julien Castel¹, Enrica Montalban¹, Ewout Foppen¹, Claire Martin¹,
6 Giulio G. Muccioli², Serge Luquet¹, Giuseppe Gangarossa¹

7
8
9
10
11
12 ¹ Université de Paris, BFA, UMR 8251, CNRS, F-75013 Paris, France

13 ² Bioanalysis and Pharmacology of Bioactive Lipids Research Group, Louvain Drug
14 Research Institute, Université catholique de Louvain, 1200 Brussels, Belgium

15
16
17
18
19 Correspondence to: giuseppe.gangarossa@u-paris.fr (GG, @PeppeGanga)

20
21
22
23
24 Key words: binge eating, dopamine, 2-AG, vagus nerve, striatum, reward,
25 metabolism

26 **Abstract (234)**

27 The regulation of food intake, a *sine qua non* requirement for survival, thoroughly
28 shapes feeding and energy balance by integrating both homeostatic and hedonic
29 values of food. Unfortunately, the widespread access to palatable food has led to the
30 development of feeding habits that are independent from metabolic needs. Among
31 these, binge eating (BE) is characterized by uncontrolled voracious eating. While
32 reward deficit seems to be a major contributor of BE, the physiological and molecular
33 underpinnings of BE establishment remain elusive. Here, we combined a
34 physiologically relevant BE mouse model with multiscale *in vivo* integrative
35 approaches to explore the functional connection between the gut-brain axis and the
36 reward and homeostatic brain structures.

37 Our results show that BE elicits compensatory adaptations requiring the gut-to-brain
38 axis which, through the vagus nerve, relies on the permissive actions of peripheral
39 endocannabinoids (eCBs) signaling. Selective inhibition of peripheral CB1 receptors
40 resulted in a vagus-dependent increased hypothalamic activity, modified metabolic
41 efficiency, and dampened activity of mesolimbic dopamine circuit, altogether leading
42 to the suppression of palatable eating. We provide compelling evidence for a yet
43 unappreciated physiological integrative mechanism by which variations of peripheral
44 eCBs control the activity of the vagus nerve, thereby in turn gating the additive
45 responses of both homeostatic and hedonic brain circuits which govern homeostatic
46 and reward-driven feeding.

47 In conclusion, we reveal that vagus-mediated eCBs/CB1R functions represent an
48 interesting and innovative target to modulate energy balance and food-reward
49 disorders.

50 **Introduction**

51

52 Feeding is a complex and highly conserved process whose orchestration results from
53 the dynamic integration of homeostatic and hedonic signals (Lutter and Nestler,
54 2009; Rossi and Stuber, 2018; Saper et al., 2002). While the firsts can be broadly
55 defined as key regulators of food intake to ensure optimal energy balance, the
56 seconds mainly relate to the reinforcing properties of sensory stimuli (perception,
57 cues, taste, odors) and reward-associated features of feeding. The homeostatic and
58 hedonic components of feeding have been respectively attributed to the
59 hypothalamic and the reward systems (Berthoud et al., 2017). However, despite the
60 well-accepted recognition that both feeding components are tightly and functionally
61 interconnected (Berthoud et al., 2017), they have usually been investigated as
62 isolated systems: homeostatic feeding vs hedonic feeding (Rossi and Stuber, 2018).
63 In addition, the counterpointing central vs peripheral regulations of feeding add a
64 supplemental degree of complexity in the identification of integrative regulatory
65 mechanisms (Coll et al., 2007; Lenard and Berthoud, 2008).

66 While energy homeostasis refers to negative feedback mechanisms maintaining the
67 body weight at set-points, the combination of both homeostatic and hedonic
68 components of feeding leads to the establishment of feed-forward mechanisms of
69 physiological adaptations. Feed-forward adaptation, also known as allostasis
70 (stability through changes), is critical in shaping energy balance and metabolic
71 efficiency (McEwen and Wingfield, 2003) but also in contributing to reward-
72 associated events (George et al., 2012; Keramati and Gutkin, 2014). Indeed, the
73 facilitated access to and the widespread consumption of palatable diets have
74 profoundly altered the delicate allostatic integration of homeostatic and hedonic
75 signals, thereby leading to the development of metabolic disorders. This is
76 particularly evident in food reward-driven dysfunctions such as binge eating (BE),
77 where the uncontrolled feeding perfectly recapitulates the efforts for an organism to
78 adapt its homeostatic processes to the hedonic aspects of feeding. In fact, short-
79 and/or long-term consumption of energy-rich palatable diets promotes dopamine
80 (DA) release from the ventral tegmental area (VTA) of the reward system (Rada et
81 al., 2005; Small et al., 2003; Wise, 2004) as well as functional adaptations within the
82 hypothalamus (Beutler et al., 2020; Linehan et al., 2020; Mazier et al., 2019; Rossi et
83 al., 2019; Wei et al., 2015). Integrative allostatic mechanisms in the hypothalamus

84 and reward systems play a major role in ensuring metabolic efficiency and
85 adaptation. Beyond these two core processors of feeding, recent reports have
86 mechanistically demonstrated that the gut-brain vagal axis, beside sensing
87 interoceptive signals and influencing feeding and energy homeostasis (Bai et al.,
88 2019; Kaelberer et al., 2018; de Lartigue, 2016), is also a major modulator of the
89 reward system (Fernandes et al., 2020; Han et al., 2016, 2018; Hankir et al., 2017;
90 Malbert et al., 2019; Tellez et al., 2013). However, the physiological processes by
91 which the gut-to-brain axis modulates reward feeding remain still unclear. Emerging
92 evidence strongly suggests that, besides a plethora of peripheral hormones (i.e.
93 ghrelin, leptin, GLP-1, CCK) (Gribble and Reimann, 2019), peripheral
94 endocannabinoids (eCBs) may be fundamental players in the regulation of feeding
95 and metabolic efficiency (Argueta and DiPatrizio, 2017; Capasso et al., 2018;
96 DiPatrizio et al., 2013; Gómez et al., 2002; Izzo et al., 2009). Indeed, eating
97 disorders-associated alterations in peripheral eCBs have been reported in obese and
98 BE patients (Monteleone et al., 2016, 2017, 2005; Quarta et al., 2011) as well as in
99 diet-induced obese rodents (Argueta and DiPatrizio, 2017; Kuipers et al., 2018).
100 However, whether and how peripheral eCBs play a permissive role in both guiding
101 reward-based feeding behaviors and buffering the allostatic regulation of energy
102 balance remain still unexplored.

103 To tackle this question, we took advantage of a physiologically relevant binge
104 eating-like mouse paradigm which, by promoting anticipatory and escalated
105 consummatory food responses, triggers reward-driven behavioral, molecular and
106 homeostatic adaptations. Binge eating, which elicited DA-dependent molecular
107 modifications in the dopaminoceptive and reward-related structures, the dorsal
108 striatum (DS) and the nucleus accumbens (NAc), revealed a yet unappreciated
109 integrative gut-to-brain orchestration requiring the modulatory actions of peripheral
110 eCBs. In particular, we show that binge eating requires an orchestrated dialog
111 between peripheral eCBs and both central hypothalamic and VTA structures through
112 the gut-brain vagal axis, thus modulating both energy balance and reward-like
113 events.

114 **Material and methods**

115

116 **Animals**

117 All experiments using animals were approved by the Animal Care Committee of the
118 Université de Paris (CEB-25–2016). 8-10 weeks old male C57Bl/6J mice (20-30
119 grams, Janvier, Le Genest St Isle, France) were single-housed one week prior to any
120 experimentation in a room maintained at 22 +/-1 °C, with light period from 7 AM to 7
121 PM. Regular chow diet (3 438 kcal/kg, protein 19%, fat 5%, carbohydrates 55%, of
122 total kcal, reference #U8959 version 63 Safe, Augy, France) and water were
123 provided *ad libitum*. *Drd2-Cre* mice (STOCK Tg(Drd2-cre) ER44Gsat/Mmucd,
124 Jackson laboratory) were used for *in vivo* fiber photometry Ca^{2+} imaging in the VTA.

125

126 **Behaviors**

127 *Palatable binge eating-like paradigm*. Intermittent daily access to the palatable
128 mixture (Intralipid 20% w/v + sucrose 10% w/v) was provided for 1 hour during 12-14
129 consecutive days at 10-11 AM in home cages. During time-locked binge sessions
130 regular chow pellets were not removed. Volume (mL) of consumed palatable mixture
131 was measured at the end of the session.

132 *Locomotor activity*. Locomotor activity (LMA) was measured in an automated online
133 measurement system using an infrared beam-based activity monitoring system
134 (Phenomaster, TSE Systems GmbH, Bad Homburg, Germany).

135 *Tail suspension*. To record the activity GCaMP6f-expressing VTA neurons, mice
136 were suspended above the ground by their tails. Ca^{2+} imaging was performed before
137 and after tail suspension.

138 *Exploratory drive in a new environment*. To record the activity GCaMP6f-expressing
139 VTA neurons in a novelty-induced exploratory drive, mice were put in a new cage
140 (NC). Ca^{2+} imaging acquisition and analysis were performed before and after
141 changing the environment.

142 *HFHS-induced increased VTA activity*. Animals were provided with a high-fat high-
143 sugar pellet to validate the recording of VTA DA-neurons (activation) in *Drd2-Cre*
144 mice. Ca^{2+} imaging acquisition and analysis were performed before and after
145 feeding.

146 *Scruff restraint*. Animals were immobilized by restraining to validate the recording of
147 VTA DA-neurons (inhibition) in *Drd2*-Cre mice. Ca^{2+} imaging acquisition and analysis
148 were performed before and after scruff restraint.

149

150 **Metabolic efficiency analysis**

151 Mice were monitored for whole energy expenditure (EE) or Heat (H), O_2 consumption
152 and CO_2 production, respiratory exchange rate ($RER=VCO_2/VO_2$, where V is a
153 volume), and locomotor activity using calorimetric cages with bedding, food and
154 water (Labmaster, TSE Systems GmbH, Bad Homburg, Germany). Ratio of gases
155 was determined through an indirect open circuit calorimeter [for review (Arch et al.,
156 2006; Even and Nadkarni, 2012)]. This system monitors O_2 and CO_2 concentration
157 by volume at the inlet ports of a tide cage through which a known flow of air is being
158 ventilated (0.4 L/min) and compared regularly to a reference empty cage. For
159 optimum analysis, the flow rate was adjusted according to the animal body weights to
160 set the differential in the composition of the expired gases between 0.4 and 0.9%
161 (Labmaster, TSE Systems GmbH, Bad Homburg, Germany). The flow was previously
162 calibrated with O_2 and CO_2 mixture of known concentrations (Air Liquide, S.A.
163 France). Oxygen consumption and carbon dioxide production were recorded every
164 15 min for each animal during the entire experiment. Whole energy expenditure (EE)
165 was calculated using the Weir equation for respiratory gas exchange measurements.
166 Food consumption was measured as the instrument combines a set of highly
167 sensitive feeding sensors for automated online measurements. Mice had access to
168 food and water *ad libitum*. To allow measurement of every ambulatory movement,
169 each cage was embedded in a frame with an infrared light beam-based activity
170 monitoring system with online measurement at 100 Hz. The sensors for gases and
171 detection of movements operated efficiently in both light and dark phases, allowing
172 continuous recording.

173 Mice were monitored for body weight and composition at the entry and the exit of the
174 experiment. Body mass composition (lean tissue mass, fat mass, free water and total
175 water content) was analyzed using an Echo Medical systems' EchoMRI (Whole Body
176 Composition Analyzers, EchoMRI, Houston, USA), according to manufacturer's
177 instructions. Briefly, mice were weighed before they were put in a mouse holder and
178 inserted in the MRI analyzer. Readings of body composition were given within 1 min.

179 Data analysis was performed on Excel XP using extracted raw values of VO_2
180 consumed, VCO_2 production (expressed in ml/h), and energy expenditure (kcal/h).

181

182 **Triglycerides, insulin and corticosterone measurements**

183 Plasma circulating triglycerides (TG) were measured with a quantitative enzymatic
184 measurement (Serum Triglyceride Determination Kit, Sigma-Aldrich, Saint-Louis,
185 USA). Insulin dosage was performed with ELISA kit (mouse ultrasensitive insulin
186 ELISA, ALPCO, Salem, NH, USA). Corticosterone was measured with RIA kit (MP
187 Biomedicals, Orangeburg, NY, USA). All kits were used according to the
188 manufacturer guidelines.

189

190 **Brown adipose tissue and telemetry body temperature measurements**

191 *Infrared camera for BAT temperature:* heat production was visualized using a high-
192 resolution infrared camera (FLIR E8; FLIR Systems, Portland, OR, USA). To
193 measure brown adipose tissue (BAT) temperature, images of interscapular regions
194 were captured before and after binge sessions. Infrared thermography images were
195 analyzed using the FLIR TOOLS.

196 *Telemetry body temperature:* telemetric devices (Data Sciences International,
197 accuracy 0.1°C) were implanted according to the manufacturer instructions. Briefly,
198 single-housed mice were anesthetized with isoflurane (1-2%) and received ip
199 injection of 10 mg/kg buprenorphine (Buprecare® 0.3 mg/ml) and 10 mg/kg
200 ketoprofen (Ketofen® 10%). The transmitter (HD-XG; Data Sciences International)
201 was placed intraperitoneally to measure longitudinal fluctuations of the core
202 temperature. After surgery, animals were allowed to recover at 35°C and received a
203 daily ip injection of ketoprofen (Ketofen® 10%) for 3 consecutive days. During a 7-
204 day recovery period, mice were carefully monitored for body weight and behavior and
205 had facilitated access to food. Implanted animals were then installed on their own
206 receiver. Data were collected using the Ponemah® software (DSI). The detection of
207 the transmitter signals was accomplished by a radio receiver (body temperature and
208 locomotor activity) and processed by a microcomputer system.

209

210 **Oral glucose tolerance test (OGTT)**

211 Oral glucose tolerance test was performed following the establishment of binge-like
212 behavior. Animals were fasted 6 hours before oral gavage of glucose (2 g/kg). Blood

213 glucose was directly measured from the vein blood tail using a glucometer (Menarini,
214 Diagnostics, Rungis, France) at 0, 15, 30, 45, 60, 90, and 120 min. Blood samples
215 were taken at 0, 15 and 30 and 60 min to measure insulin levels. Insulin dosage was
216 performed with ELISA kit (mouse ultrasensitive insulin ELISA (ALPCO, Salem, NH,
217 USA), according to the manufacturer guidelines).

218

219 **Tissue preparation and immunofluorescence**

220 For immunohistochemistry, animals were injected with i.p. pentobarbital (500 mg/kg,
221 i.p., Sanofi-Aventis, France). Once anaesthetized, animals were transcardially
222 perfused with 4°C PFA 4% for 5 minutes. Brains were collected, put overnight in PFA
223 4% and then stored in PBS, 4°C. 30 µm-thick sections were sliced with a vibratome
224 (Leica VT1000S, France), and stored in PBS 4°C. Sections were processed as
225 follows: Day 1: free-floating sections were rinsed in Tris-buffered saline (TBS; 0.25 M
226 Tris and 0.5 M NaCl, pH 7.5), incubated for 5 min in TBS containing 3% H₂O₂ and
227 10% methanol, and then rinsed three times for 10 min each in TBS. After 15 min
228 incubation in 0.2% Triton X-100 in TBS, sections were rinsed three times in TBS
229 again. Slices were then incubated overnight or 48 hrs at 4°C with the following
230 primary antibodies: rabbit anti-phospho-rpS6 Ser^{235/236} (1:1000, Cell Signaling
231 Technology, #2211), rabbit anti-phospho-rpS6 Ser^{240/244} (1:1000, Cell Signaling
232 Technology, #2215), rabbit anti-cFos (1:1000, Synaptic Systems, #226 003) or
233 mouse anti-TH (1:1000, Millipore, #MAB318). Sections were rinsed three times for 10
234 min in TBS and incubated for 60 min with second anti-rabbit Cy3 AffiniPure (1:1000,
235 Jackson Immunoresearch). Sections were rinsed for 10 min twice in TBS and once in
236 TB (0.25 M Tris) before mounting.

237 Acquisitions were performed with a confocal microscope (Zeiss LSM 510). Images
238 used for quantification were all single confocal sections. The objectives and the
239 pinhole setting remained unchanged during the acquisition of a series for all images.
240 Quantification of immunoreactive cells was performed using the cell counter plugin of
241 the ImageJ software taking as standard reference a fixed threshold of fluorescence.

242

243 **Western blotting**

244 At the end of the binge session, the mouse head was cut and immediately immersed
245 in liquid nitrogen for 3 seconds. The brain was then removed and dissected on ice-
246 cold surface, sonicated in 200 µl (dorsal striatum) and 100 µl (nucleus accumbens) of

247 1% SDS supplemented with 0.2% phosphatase inhibitors and 1% protease inhibitors,
248 and boiled for 10 minutes. Aliquots (2.5 μ l) of the homogenates were used for protein
249 quantification using a BCA kit (BC Assay Protein Quantitation Kit, Interchim Uptima,
250 Montluçon, France). Equal amounts of proteins (10 μ g) supplemented with a Laemli
251 buffer were loaded onto 10% polyacrylamide gels. Proteins were separated by SDS-
252 PAGE and transferred to PVDF membranes (Millipore). The membranes were
253 immunoblotted with the following antibodies: rabbit anti-phospho-Ser^{235/236}-rpS6
254 (1:1000, Cell Signaling Technology, #2211), rabbit anti-phospho-Ser^{240/244}-rpS6
255 (1:1000, Cell Signaling Technology, #2215), rabbit anti-phospho-ERK (1:2000, Cell
256 Signaling Technology, #4370), mouse anti-beta-actin (1:5000, Sigma Aldrich,
257 #A1978). Detection was based on HRP-coupled secondary antibody binding using
258 ECL. The secondary antibodies were anti-mouse (1:5000, Dako, #P0260) and anti-
259 rabbit (1:10000, Cell Signaling Technology, #7074). Membranes were imaged using
260 the Amersham Images 680. Quantifications were performed using the ImageJ
261 software.

262

263 **Drug treatments**

264 The following compounds were used: insulin (0.5 U/kg, Novo Nordisk, Lot GT67422),
265 CCK-8S (10 μ g/kg, Tocris, #1166), liraglutide (100 μ g/kg, gift from Novo Nordisk),
266 exendin 4 (10 μ g/kg, Tocris, #1933), leptin (0.25 mg/kg, Tocris, #2985), AM251 (3
267 mg/kg, Tocris, #1117), AM6545 (10 mg/kg, Tocris, #5443), SKF81297 (5 mg/kg,
268 Tocris, #1447), haloperidol (0.25 and 0.5 mg/kg, Tocris, #0931), SCH23390 (0.1
269 mg/kg, Tocris, #0925), GBR12909 (10 mg/kg, Sigma Aldrich, #D052), d-
270 amphetamine sulphate (2 mg/kg, Tocris, #2813), JZL184 (8 mg/kg, Tocris, #3836).

271

272 **Subdiaphragmatic vagotomy**

273 Prior to surgery and during 3 post-surgery days, animals were provided with *ad*
274 *libitum* jelly food (DietGel Boost Clear H₂O) to avoid the presence of solid food in the
275 gastrointestinal tract. Animals received Buprécare® (Buprenorphine 0.3 mg) diluted
276 1/100 in NaCl 0.9% and Ketofen® (Ketoprofen 100 mg) diluted 1/100 in NaCl 0.9%
277 and were anaesthetized with 3.5% isoflurane for induction and 1.5% for maintenance
278 during the surgery. Their body temperature was maintained at 37°C. Briefly, using a
279 binocular microscope, the right and left vagus nerve branches were carefully isolated
280 along the esophagus and sectioned in vagotomized animals or left intact in sham

281 animals. Mice spent at least 3 weeks of post-surgery recovery period before being
282 used for the experimental procedures.

283

284 **Quantification of plasma eCBs**

285 Blood was collected before and after the last binge session and immediately
286 centrifuged to isolate the plasma. Plasma (50 μ L) was added to vials containing
287 dichloromethane (8 mL), methanol (MeOH, 4 mL) (containing BHT), water
288 (containing EDTA) and the internal standards (deuterated *N*-acylethanolamines,
289 deuterated 2-AG). Following extraction, the lipid-containing fraction was purified by
290 solid phase extraction (SPE). The endocannabinoids and related NAEs were
291 recovered from the SPE column using hexane-isopropanol 7:3 (v/v) and transferred
292 to injection vials (Bottemanne et al., 2019). The samples (1 μ L) were analyzed using
293 an Acquity UPLC® class H coupled to a Xevo TQ-S mass spectrometer (both from
294 Waters). For the separation we used an Acquity UPLC® BEH C18 (2.1x50 mm; 1.7
295 μ m, 40°C) column and a gradient (200 μ L/min) between MeOH-H₂O-acetic acid
296 (75:24.9:0.1; v/v/v) and MeOH-acetic acid (99.9:0.1; v/v). Ionization was obtained
297 using an ESI source operated in the positive mode. A quantification and a
298 qualification transition were optimized for each analyte and MassLynx® used for data
299 acquisition and processing. For each analyte, the ratio between the AUC of the lipid
300 and the AUC of the corresponding internal standard was used for data normalization.
301 Calibration curves were obtained in the same conditions.

302

303 **Viral production**

304 pAAV.Syn.Flex.GCaMP6f.WPRE.SV40 (titer $\geq 1 \times 10^{13}$ vg/ml, working dilution 1:5)
305 was a gift from Douglas Kim (Addgene viral prep #100833-AAV9;
306 <https://www.addgene.org/100833/>; RRID:Addgene_100833).

307

308 **Stereotaxic procedure**

309 Mice were anaesthetized with isoflurane and received 10 mg/kg intraperitoneal
310 injection (i.p.) of Buprécare® (Buprenorphine 0.3 mg) diluted 1/100 in NaCl 0.9% and
311 10 mg/kg of Ketofen® (Ketoprofen 100 mg) diluted 1/100 in NaCl 0.9%, and placed
312 on a stereotaxic frame (Model 940, David Kopf Instruments, California).
313 pAAV.Syn.Flex.GCaMP6f.WPRE.SV40 (0.3 μ l) was injected unilaterally (for fiber
314 photometry) into the ventral tegmental area (VTA) (L=-0.5; AP=-3.4; V=-4.4, mm) of

315 *Drd2*-Cre mice at a rate of 0.05 μ l/min. The injection needle was carefully removed
316 after 5 minutes waiting at the injection site and 2 minutes waiting halfway to the top.
317 Optical fiber for calcium imaging into the VTA was implanted 100 μ m above the viral
318 injection site. Animals were tested 4 weeks after viral stereotaxic injections.

319

320 **Fiber photometry and data analysis**

321 A chronically implantable cannula (Doric Lenses, Québec, Canada) composed of a
322 bare optical fiber (400 μ m core, 0.48 N.A.) and a fiber ferrule was implanted 100 μ m
323 above the location of the viral injection site in the ventral tegmental area (VTA:
324 L=+/-0.5; AP=-3.4; V=-4.4, mm). The fiber was fixed onto the skull using dental
325 cement (Super-Bond C&B, Sun Medical). Real-time fluorescence signals emitted
326 from the calcium indicator GCaMP6f expressed by D2R-containing VTA neurons
327 were recorded and analyzed as previously described (Lerner et al., 2015).
328 Fluorescence was collected in the VTA using a single optical fiber for both delivery of
329 excitation light streams and collection of emitted fluorescence.

330 The fiber photometry setup used 2 light-emitting LEDs: 405 nm LED sinusoidally
331 modulated at 330 Hz and a 465 nm LED sinusoidally modulated at 533 Hz (Doric
332 Lenses) merged in a FMC4 MiniCube (Doric Lenses) that combines the 2
333 wavelengths excitation light streams and separate them from the emission light. The
334 MiniCube was connected to a Fiberoptic rotary joint (Doric Lenses) connected to the
335 cannula. A RZ5P lock-in digital processor controlled by the Synapse software
336 (Tucker-Davis Technologies, TDT, USA), commanded the voltage signal sent to the
337 emitting LEDs via the LED driver (Doric Lenses). The light power before entering the
338 implanted cannula was measured with a power meter (PM100USB, Thorlabs) before
339 the beginning of each recording session. The irradiance was \sim 9 mW/cm². GCaMP6f-
340 emitted fluorescence was collected by a femtowatt photoreceiver module (Doric
341 Lenses) through the same fiber patch cord. The signal was then received by the
342 RZ5P processor (TDT). On-line real-time demodulation of the fluorescence due to
343 the 405nm and the 465 nm excitations was performed by the Synapse software
344 (TDT). A camera was synchronized with the recording using the Synapse software.
345 Signals were exported to Python 3.0 and analyzed off-line using TDT Python SDK
346 packages.

347 For the new cage paradigm, signal analysis was performed on two-time intervals:
348 one extending from –60 to 0 seconds (home cage, HC) and the other from 0 to 60
349 seconds (new cage, NC).

350 For the tail suspension paradigm, signal analysis was performed on two-time
351 intervals: one extending from –60 to 0 seconds (baseline) and the other from 0 to 120
352 seconds (tail suspension).

353 $\Delta F/F$ was calculated as $[(465 \text{ nm signal}_{\text{test}} - \text{fitted } 405 \text{ nm signal}_{\text{ref}})/\text{fitted } 405 \text{ nm}$
354 $\text{signal}_{\text{ref}}]$. To compare signal variations between the two conditions (NC vs HC or tail
355 suspension vs baseline) for each mouse a difference between AUCs ($\text{AUC}_2 - \text{AUC}_1$)
356 was used.

357

358 **Statistics**

359 Data are presented as mean \pm SEM. All statistical tests were performed with Prism 6
360 (GraphPad Software, La Jolla, CA, USA). The detailed statistical analyses are listed
361 in the Supplementary Table 1. Depending on the experimental design, data were
362 analyzed using either Student t-test (paired or unpaired) with equal variances, One-
363 way ANOVA or Two-way ANOVA. In all cases, the significance threshold was
364 automatically set at $p < 0.05$. ANOVA analyses were followed by Bonferroni *post hoc*
365 test for specific comparisons only when overall ANOVA revealed a significant
366 difference (at least $p < 0.05$).

367 **Results**

368

369 **Time-locked access to palatable diet induces adaptation of nutrient partitioning**
370 **and metabolic efficiency**

371 Several preclinical paradigms of bingeing are widely used to model humans' eating
372 disorders (Avena, 2010). However, the majority of currently available paradigms
373 mainly rely on (i) prior alterations of basal homeostasis (food or water
374 restriction/deprivation, stress induction), (ii) dietary exposure to either high-sugar or
375 high-fat foods or (iii) the absence of food choice during bingeing periods.

376 We therefore adapted existing protocols to better study reward and homeostatic
377 components of food intake during binge eating (BE). In our protocol, since dietary
378 mixtures of fat and sugar lead to enhanced food reward properties (DiFeliceantonio
379 et al., 2018), a highly palatable milkshake (sugar and fat) was designed to promote
380 intense craving and reward-driven feeding. Time-locked access to this milkshake was
381 sufficient to drive escalating binge-like consumption with no need of restricting
382 access to chow diet (**Figure 1A**). In that regard, we are confident that our BE model
383 is preferentially driven by reward values over metabolic demands since animals are
384 neither food nor water restricted.

385 Mice intermittently exposed to this dietary palatable mixture rapidly maximized their
386 intake within a few days, reaching an averaged consumption of 1.4 mL in 1h (~3.4
387 kcal/h) (**Figure 1B**). Importantly, intermittent (1h/day) exposure to palatable non-
388 caloric sucralose or saccharin solutions did not lead to escalating binge-like
389 consumption (**Suppl. Figure 1A, B**), indicating that calorie content, beyond taste
390 perception itself, is necessary to drive incentive salience and BE-like behavior.

391 This palatable food consumption was simultaneously associated with an increased
392 anticipatory locomotor activity ~2 hours before food access and lasted for another
393 ~1-2 hours following access (**Figure 1C, C¹**), with no changes in the ambulatory
394 activity during the dark phase (**Figure 1C**). The same animals were characterized by
395 a significant reduction in spontaneous nocturnal food intake (**Figure 1D, D¹**).
396 However, in bingeing animals the overall calories intake [standard diet (SD) +
397 palatable food (PF)] remained identical to controls, thus indicating a conserved
398 isocaloric maintenance in calories consumption despite reward-driven food intake
399 (**Figure 1E**). Importantly, isocaloric feeding was associated with conserved body
400 weight (BW) and body composition during the experimental protocol (**Figure 1F,**

401 **Suppl. Figure 1C, D).** Next, we investigated the consequence of palatable food
402 exposure and BE progression onto metabolic efficiency. Indirect calorimetry analysis
403 revealed an increase in the respiratory exchange ratio (RER) before and after
404 intermittent palatable food consumption (**Figure 1G, G¹**), and a stark reduction was
405 detected in the dark phase (**Figure 1G**), thereby highlighting a metabolic shift of
406 energy substrates use (from carbohydrates to lipids as indicated by RER ~1 or RER
407 ~0.7 respectively). Such metabolic shift toward lipid substrates was further confirmed
408 by the modulation of fatty acids oxidation (FAO, **Suppl. Figure 1E**). In addition, we
409 also observed an increase in energy expenditure (EE) during the food anticipatory
410 and consummatory phases (**Figure 1H, H¹**). Furthermore, infrared thermography
411 analysis revealed that BE was associated with a transient increase in brown adipose
412 tissue (BAT) energy dissipation (**Figure 1I**) while telemetric recording of core body
413 temperature revealed a BE specific increase during the anticipatory, consummatory
414 and post-prandial phases (**Figure 1J, J¹, Suppl. Figure 1F**) and a sharp reduction
415 during the last hours of the dark phase in BE animals. Overall, changes in core body
416 temperature were fostered around the time of time-locked palatable food access and
417 overlapped with the increase in locomotor activity (**Figure 1J, K**).

418 Access to calories-rich food and time-restricted feeding are invariably associated with
419 changes in circulating signals reflecting metabolic and behavioral adaptations
420 (Oosterman et al., 2020). In line with this, we observed that our model of BE was
421 associated with reduced circulating triglycerides (TG) and insulin and concomitant
422 increase in circulating corticosterone during the anticipatory phase (**Figure 2A-C**)
423 while overall insulin sensitivity, as assessed by oral glucose tolerance test, remained
424 unchanged (**Figure 2D, E**). These data support the notion that homeostatic
425 adaptations occurring during time-locked palatable feeding lead to changes in lipid-
426 substrates utilization and promotes adaptive activation of the hypothalamic-pituitary-
427 adrenal (HPA) axis.

428 Overall, these results point to a rapid allostatic adaptation of metabolic and
429 behavioral readouts, during which animals optimize their palatable food consumption
430 and physiologically adapt by compensating the time-locked calories load to maintain
431 a stable body weight.

432

433 **BE induces dopamine-related modifications in a D1R-dependent manner**

434 Dopamine (DA) neurons and DA-sensitive structures, such as the dorsal striatum
435 (DS) and the nucleus accumbens (NAc), are critical players in reward-based
436 paradigms but also in BE disorders (Balodis et al., 2015; Palmiter, 2007; Spierling et
437 al., 2020; Wang et al., 2011). Here, we investigated whether bingeing modulated the
438 DA-associated signaling machinery. Thus, we used the activation (phosphorylation)
439 of the ribosomal protein S6 (rpS6) and the extracellular signal-regulated kinases
440 (ERK) as functional readouts of DA-dependent molecular activity (Gangarossa et al.,
441 2013a, 2013b, 2019; Valjent et al., 2019). We first investigated such molecular
442 activations in bingeing mice before and after reward-diet consumption (**Figure 3A**) in
443 the DS and NAc (**Figure 3B**).

444 The food anticipatory phase was associated with an increase in ERK activation only
445 in the DS (**Figure 3C, D**), mostly reflecting the increased locomotor activity during the
446 anticipatory phase. Importantly, palatable food consumption induced an increase in
447 phospho-ERK and phospho-rpS6 (at both Ser^{235/236} and Ser^{240/244} sites) in both DS
448 and NAc (**Figure 3C-E**). Interestingly, acute (single) consumption of palatable diet
449 failed in triggering ERK and rpS6 activation (**Figure 3C-E**), thus revealing that
450 molecular adaptation of the DA signaling in the DS/NAc are tightly dependent on the
451 full establishment of the binge behavior and not only on the consumption of the
452 palatable food. Immunofluorescence analysis revealed that BE-induced rpS6
453 activation was clearly evident in the DS and NAc (**Figure 3F, G**).

454 Next, we wondered whether food-reward anticipatory and/or consummatory
455 phases were followed by adaptive changes in DA-evoked behavioral responses.
456 Thus, we treated mice with GBR12909 (10 mg/kg), a specific dopamine transporter
457 (DAT) blocker that prevents the presynaptic reuptake of DA, ultimately leading to its
458 accumulation into the synaptic cleft. Interestingly, we observed a different behavior
459 depending on BE phases (anticipatory vs consummatory). Before palatable food
460 access, GBR treatment increased locomotor activity in both bingeing and control
461 animals (**Figure 4A, A¹**). However, when GBR was administered following palatable
462 food consumption (1h), GBR-induced locomotor response was blunted in bingeing
463 animals (**Figure 4B, B¹**). These results indicate that BE-induced physiological
464 adaptations are characterized by the enabled ability for palatable food to impinge on
465 DA release and action. At the postsynaptic level, DA acts onto medium spiny
466 neurons (MSNs) which express either the dopamine D1R (D1R-MSNs) or D2R (D2R-
467 MSNs). In order to discriminate the role of D1R vs D2R signaling in BE, we

468 pretreated animals with the D1R antagonist SCH23390 (0.1 mg/kg) or vehicle (Veh)
469 before providing access to palatable diet. SCH23390 dramatically reduced palatable
470 food consumption (**Figure 4C**). On the contrary, pretreatment with haloperidol (0.25
471 and 0.5 mg/kg) did not dampen palatable food consumption (**Figure 4D**), even at
472 doses (0.5 mg/kg) known to trigger cataleptic responses (Kobayashi et al., 1997;
473 Radl et al., 2018). This evidence suggests that loss of control on palatable bingeing
474 primarily relies on D1R signaling. In line with this event, activation of striatal D1R
475 leads to downstream phosphorylation of rpS6 and ERK (Biever et al., 2015;
476 Gangarossa et al., 2013a). Importantly, the adaptive molecular changes in the DS
477 and NAc also required D1R activation since SCH23390 (0.1 mg/kg) largely
478 suppressed BE-associated phosphorylations of rpS6 in both DS (**Figure 4E**) and
479 NAc (**Figure 4F**). These results indicate that D1R is critical in driving palatable food
480 consumption and its associated molecular activations in the specific context of BE. Of
481 note, although SCH23390 reduced anticipatory locomotor activity in pretreated
482 animals, basal locomotor activity in naive animals was not impaired (**Figure 4G, G¹**),
483 thereby excluding the confounding effects due to changes in basal locomotor activity.
484 Furthermore, a compensatory rescue in chow intake was observed in SCH23390-
485 pretreated bingeing animals during the dark phase, excluding potential long-lasting
486 effects of the D1R inhibition (**Figure 4H**). To further validate the hypothesis that D1R
487 may be involved in BE-elicited dopamine modifications, we measured the locomotor
488 activity triggered by the activation of D1R with its direct agonist SKF81297 (5 mg/kg)
489 at the end of the BE session (1h after food access). At the end of the session, the
490 D1R agonist SKF81297 (5 mg/kg) was administered to control and bingeing animals.
491 Interestingly, we observed an earlier (first 30 min) significant increase in locomotor
492 activity in bingeing animals compared to control mice (**Figure 4I, I¹**), although no
493 major differences were detected during the cumulative 2-hrs response (**Figure 4I¹**).
494 Overall, our results reveal that the critical phases surrounding palatable food
495 consumption in the context of BE profoundly affect DA-associated signaling and
496 promote consummatory and behavioral responses that primarily rely on D1R-
497 dependent signaling.

498

499 **Peripheral endocannabinoids govern binge eating**

500 Recent studies have highlighted the role of enteric neuronal and endocrine systems
501 in the regulation of food reward-seeking and DA-associated behaviors (de Araujo et

502 al., 2020; Reichelt et al., 2015). We therefore tested whether gut-born metabolic
503 signals had a privileged action onto BE-like consumption of palatable diet when
504 compared to other known circulating satiety signals.

505 Firstly, we observed that peripherally injected leptin (0.25 mg/kg), or insulin
506 (0.5 U/kg), did not trigger any reduction in palatable food consumption when injected
507 in bingeing animals (**Figure 5A**). Then, we investigated whether gut-born satiety
508 signals retained anorectic properties with a similar protocol. Glucagon-like peptide
509 hormone (GLP-1) is a satiety signal produced by the endocrine cells of the intestine.
510 GLP-1R agonists, exendin-4 and liraglutide, are known to decrease food intake
511 (Ladenheim, 2015). Both GLP-1 mimetic drugs (exendin-4, 10 µg/kg and liraglutide,
512 100 µg/kg) successfully reduced binge-consumption of palatable diet (**Figure 5A**).
513 Similarly, the cholecystokinin (CCK) analog CCK-8S (10 µg/kg) acutely decreased
514 palatable food intake (**Figure 5A**).

515 These results indicate that dietary-induced BE is associated with the resistance to
516 the satiety action of leptin and insulin, while the anorectic action of gut-born signals
517 remains unaltered.

518 Bioactive lipids, among which endocannabinoids (eCBs), are important signals to
519 relay nutrients-induced adaptive responses in the gut-brain axis (DiPatrizio and
520 Piomelli, 2015; Lau et al., 2017). Therefore, we explored the plasticity and functions
521 of eCBs signaling in dietary-induced BE.

522 First, we pharmacologically inhibited the CB1R with the selective inverse agonist
523 AM251 (3 mg/kg). Blockade of CB1R dramatically reduced BE-like consumption
524 (**Figure 5A**). Next, we wondered whether bingeing was accompanied by alterations
525 in circulating peripheral eCBs [anandamide (AEA) and 2-arachidonoylglycerol (2-
526 AG)] and eCBs-related species [docosahexanoyl ethanolamide (DHEA),
527 oleoylethanolamide (OEA)]. While circulating *N*-acylethanolamines (AEA, DHEA,
528 OEA) remained unaffected, time-locked palatable feeding induced a significant
529 increase in 2-AG immediately after food consumption (**Figure 5B**).

530 Since the CB1R is highly expressed in both peripheral and central nervous
531 systems, we were eager to distinguish the respective contribution of central or
532 peripheral of CB1R signaling in BE outputs. Thus, we used the peripherally restricted
533 CB1R neutral antagonist AM6545 (10 mg/kg, i.p.), a compound unable to cross the
534 blood brain barrier (Boon et al., 2014; Cluny et al., 2010; Tam et al., 2010).
535 Pretreatment with AM6545 (10 mg/kg, 1h before palatable-food access) induced a

536 stark abolishment of BE consumption when administered acutely (**Figure 5C**).
537 Conversely, the increase of circulating eCB achieved through the pharmacological
538 inhibition (JZL184, 8 mg/kg) of the enzyme responsible of 2-AG hydrolysis, the
539 monoacylglycerol lipase (MAGL) (Long et al., 2009), resulted in an increase of
540 palatable food consumption that was fully prevented by AM6545 (**Figure 5C**). This
541 bidirectional modulatory action of eCBs/CB1R onto BE did not show signs of
542 desensitization and remained efficient throughout 4 days of daily pharmacological
543 intervention (**Figure 5D**). In the same line, thermogenic and locomotor activity
544 analyses revealed that pretreatment with AM6545 strongly dampened both the
545 anticipatory and consummatory phases of BE (**Figure 5E, F**).
546 These results indicate that peripheral CB1R signaling is sufficient to control
547 compulsive eating in BE.

548

549 We next explored how peripheral CB1R signaling modulates metabolic
550 efficiency in the context of BE. Pretreatment with AM6545 (10 mg/kg, i.p.)
551 significantly increased fatty acid oxidation (FAO) (**Figure 5G, G¹**). Importantly, this
552 AM6545-induced increased FAO did not depend neither on reduced calorie intake
553 (Binge session) or basal calorie contents (NoBinge session) (**Figure 5G²**) nor on
554 altered energy expenditure (EE) (**Suppl. Figure 2A**).

555 These results indicate that acute manipulation of peripheral, brain-excluded, eCB
556 tone affects nutrient partitioning and promotes a shift towards whole body lipid-
557 substrate utilization.

558 Importantly, we observed neither blunted palatable feeding responses (**Figure 5H**)
559 nor increased FAO (**Figure 5I**) when AM6545 was orally (p.o.) administered. These
560 results suggest that, in our behavioral model, CB1R-mediated homeostatic
561 adaptations do not depend on the lumen-oriented apical CB1R expression in
562 endothelial or enteroendocrine intestinal cells (Argueta et al., 2019; Sykaras et al.,
563 2012) but rather on non-lumen-oriented CB1R. Recent reports have indicated that
564 CB1R is also expressed in vagal afferent neurons (Burdyga et al., 2010; Egerod et
565 al., 2018). To discriminate between all vagal afferents, we performed a meta-analysis
566 on recent single-cell transcriptomic results (Bai et al., 2019) obtained through a path-
567 specific viral strategy of gut segments (**Figure 5J**). This analysis revealed, that *Cnr1*
568 (gene encoding for CB1R), but not *Cnr2*, was highly enriched in all segments of the
569 gut-brain vagal axis (**Figure 5K, Suppl. Figure 2B, C**) and that, together with well-

570 known afferent markers (*Slc17a6*, *Scn10a*, *Htr3a*, *Cartpt*, *Grin1*, *Phox2b*), *Cnr1* may
571 be considered as a constitutive marker of vagal sensory neurons.

572

573 **The gut-brain vagal axis is required for eCBs-mediated effects**

574 We have shown that gut-brain satiety signals and peripheral CB1R signaling retained
575 full anorectic potency while circulating signals, leptin and insulin, failed to decrease
576 feeding in our BE model (**Figure 5**). Given that peripheral eCBs can mediate their
577 action in part through the vagus nerve (Bellocchio et al., 2013) this result strongly
578 supports a critical implication for gut-born nervous inputs in the
579 establishment/maintenance of BE-like behavior. Thus, we took advantage of
580 subdiaphragmatic gut vagotomy (VGX) to investigate whether the eCBs-vagus axis
581 was necessary/sufficient to mediate the anti-bingeing effects. In sham mice, injection
582 of the peripherally restricted CB1R antagonist AM6545 led to a strong increase in
583 cFos-expressing neurons in the nucleus tractus solitarius (NTS) and the area
584 postrema (AP) while the signal was fully abolished in vagotomized mice (**Figure 6A**,
585 **A¹**, **A²**). In addition, we observed a vagus-dependent increase in cFos also in the
586 NTS-projecting lateral parabrachial nucleus (IPBN) (**Figure 6A**), indicating that
587 peripheral modulation of eCB action influences central brain pathways.

588 We also observed that the integrity of the vagus nerve was essential to mediate the
589 anorectic action of AM6545 on BE behavior (**Figure 6B**). Importantly, although
590 vagotomy (VGX) *per se* was associated with a decrease in time-locked hedonic
591 feeding and consequent BE-derived compensatory homeostatic adaptations (**Suppl.**
592 **Figure 3**), peripheral CB1R antagonist did not trigger an additive anorectic response
593 (**Figure 6B**) in VGX mice compared to sham mice. Furthermore, vagotomy abolished
594 the increase in FAO following AM6545 administration observed in sham mice (**Figure**
595 **6C**, **C¹**, **6D**, **D¹**). These results demonstrate that the gut-brain vagal communication
596 routes feeding and the metabolic components associated with BE.

597 These vagus-dependent homeostatic adaptations promoted by peripheral blockade
598 of CB1R prompted us to investigate whether AM6545 was able to alter the activity of
599 brainstem-projecting central structures that control feeding. Indeed, AM6545 induced
600 a strong vagus-dependent increase of cFos-neurons in the hypothalamic regions
601 PVN and DMH (**Figure 6E**, **E¹**, **F**, **F¹**), thereby indicating that the metabolic
602 adaptations induced by peripheral blockade of CB1R require a vagus-mediated
603 NTS→PBN→hypothalamus circuit whose nodes' activation control feeding and

604 energy homeostasis (Cheng et al., 2020; D'Agostino et al., 2016; Grill and Hayes,
605 2012).

606

607 **Peripheral CB1R signaling routed by the vagus nerve controls the activity of** 608 **VTA dopamine neurons**

609 Since palatable bingeing also strongly relies on central DA-dependent mechanisms
610 (**Figure 3, 4**), we therefore explored the functional connection between peripheral
611 eCBs and gut-to-brain vagal axis in the modulation of the reward DA system. Naive
612 mice were pretreated with AM6545 (10 mg/kg, i.p.) or vehicle before being
613 administered with the DAT blocker GBR12909 (10 mg/kg). Blockade of peripheral
614 CB1R drastically reduced GBR-induced locomotor activity (**Figure 7A, A¹**) as well as
615 GBR-triggered cFos induction in the striatum (**Figure 7B, B¹**). Interestingly, AM6545
616 failed in contrasting amphetamine-induced locomotor activity (**Figure 7C**), thereby
617 suggesting that inhibition of peripheral CB1R may modulate the intrinsic activity of
618 DA-neurons rather than altering evoked DA release events.

619 These results reveal that inhibition of peripheral CB1R, besides promoting satiety
620 and FAO, may dampen reward-driven feeding also by concomitantly reducing DA-
621 neurons activity and consequent activation of the dopaminoceptive structures.

622 To directly address this point, VGX mice were pretreated with AM6545 prior to
623 receiving GBR12909. Remarkably, ablation of the vagus nerve prevented AM6545-
624 induced blunting of GBR-elicited locomotor activity (**Figure 7D, D¹**). Moreover, this
625 vagus-to-brain effect was further highlighted by the lack of action of AM6545 when
626 orally administered (**Figure 7E, E¹**), as reported for palatable bingeing (**Figure**
627 **5H**). When AM6545 was primarily contained to the lumen and epithelial surface of
628 the gut through oral administration, no effects on GBR-mediated hyperlocomotion
629 were observed.

630 This result supports the notion that the modulatory action of peripheral eCB signaling
631 onto the gut-brain axis in controlling reward BE is located outside of gut lumen.

632 Finally, to fully establish that peripheral inhibition of CB1R modulates the activity of
633 dopamine VTA neurons, we performed cell type-specific *in vivo* Ca²⁺ imaging of DA-
634 neurons in presence or absence of AM6545. We took advantage of the *Drd2-Cre*
635 mouse line to express virally mediated GCaMP6f in VTA DA-neurons (**Figure 7F**)
636 since they co-express the autoreceptor D2R (Anzalone et al., 2012; Usiello et al.,
637 2000). Indeed, using this mouse line we were able to detect activation and inhibition

638 of VTA DA-neurons following rewarding (high-fat high-sugar pellet) or aversive (scruff
639 restraint) events (**Suppl. Figure 4A, B**), respectively. To trigger the activity of DA-
640 neurons independently from food- or drugs-associated stimuli, we used two
641 paradigms that modulate DA-neurons activity: exposure to a new environment
642 (Takeuchi et al., 2016) which promotes exploration and tail suspension (Kolata et al.,
643 2018) (**Figure 7G**). Importantly, inhibition of peripheral CB1R (AM6545) led to a
644 reduced activation of VTA DA-neurons in both paradigms (**Figure 7H, I**), thus
645 revealing that peripheral CB1R lead to the abolishment of BE through the activation
646 of satietogenic (**Figure 5, 6**) and the inhibition of reward circuits (**Figure 7**).

647 **Discussion**

648

649 A characteristic feature of feeding behavior is its key ability to dynamically adapt to
650 sensory and environmental stimuli signaling food availability. Such adaptive strategy
651 is even more pronounced when food is palatable and energy-dense. Indeed, the
652 control of feeding strategies requires complex and highly interacting systems that can
653 hardly be unequivocally attributed to single structures or circuits.

654 In our study, by using *in vivo* integrative approaches, we observed that, first,
655 palatable time-locked feeding mobilizes both homeostatic and hedonic components
656 of feeding through fast, but yet physiological, allostatic adaptations. Second, such
657 allostatic adaptations require a concerted involvement of central DA (hedonic drive)
658 and peripheral eCBs signaling (homeostatic and hedonic drive). Third, the permissive
659 role of peripheral eCBs fully relies on the vagus nerve which, by a polysynaptic
660 circuit, controls the activity of both satietogenic and reward (dopamine) structures.
661 Fourth, our results point to peripheral CB1R neutral antagonists as promising
662 therapeutic tools to counteract eating as well as reward-related disorders.

663 Overall, our study describes for the first time the fundamental role of eCB/vagal gut-
664 brain transmission as a core component of binge eating and its behavioral, cellular
665 and molecular adaptations.

666

667 Here, by investigating the pathways involved in hedonic feeding in absence of
668 induced hunger or energy deprivation, we provide evidence that the hedonic drive to
669 eat, as triggered by our intermittent time-locked model, promotes rapid homeostatic
670 compensations leading to escalating consumption of palatable food and to allostatic
671 adaptations of energy metabolism. As such, caloric demands are fulfilled and
672 classical energy-mediated homeostatic signals (leptin, insulin) do not seem to
673 spontaneously interfere, thus providing us the opportunity to study food intake-related
674 integrative pathways with the abstraction of the homeostatic vs hedonic discrepancy.
675 In line with clinical data (Carr and Grilo, 2020; Hutson et al., 2018), we observed that
676 binge-like feeding in lean animals is not necessarily associated with overweight gain
677 and does not lead to disrupted body weight homeostasis. On the contrary, through an
678 allostatic feed-forward mechanism, mice rapidly adapt to palatable food availability by
679 reducing their nocturnal feeding patterns in order to maximize time-locked (1h)
680 hedonic feeding. Such adaptations, ranging from increased anticipatory feeding

681 phase to pre-feeding increased corticosterone levels and food intake maximization,
682 all represent key hallmarks of the compulsive and emotional states of BE patients
683 (Bake et al., 2014; Muñoz-Escobar et al., 2019; Naish et al., 2019). The anticipatory
684 feeding phase was associated with decreased levels of plasma TG and insulin,
685 whereas both anticipatory and consummatory phases were characterized by
686 increased energy expenditure, core temperature and metabolic efficiency, thereby
687 suggesting a metabolic shift of nutrients' use. This observation perfectly mirrors the
688 allostatic theory, which stands on the fact that an organism anticipates and adapts to
689 environmental changes while accordingly adjusting several physiological parameters
690 to maintain stable physiological states (De Ridder et al., 2016; Ramsay and Woods,
691 2014). Allostatic mechanisms have classically been discussed in terms of stress-
692 related regulatory events. However, the hedonic value of a stimulus (food,
693 recreational drugs) can function as a feed-forward allostatic factor (George et al.,
694 2012).

695

696 During time-locked palatable feeding, such allostatic adaptations (anticipation
697 and consumption of palatable food) required intact DA signaling. In fact, analysis of
698 key DA-activated downstream phospho-targets in the DS and NAc highlighted
699 specific patterns of molecular activation. Notably, while the anticipatory phase was
700 associated with an increase in ERK and rpS6^{Ser235/236} phosphorylations, the
701 consummatory phase was also accompanied by a robust increase in mTOR-
702 mediated rpS6^{Ser240/244} activation. Such signaling events, which did not depend on a
703 single episode of palatable food intake, required the dopamine D1R as administration
704 of SCH23390, but not of the D2R antagonist haloperidol, prevented binge-like
705 behavior and its associated molecular modifications. This is of interest since, contrary
706 to the well-known molecular insights of drugs of abuse which require the D1R
707 (Bertran-Gonzalez et al., 2008; Gore and Zweifel, 2013; Kai et al., 2015; Luo et al.,
708 2011; Sutton and Caron, 2015), food-related disorders have usually been
709 predominantly associated with altered D2R signaling (Caravaggio et al., 2015; Kenny
710 et al., 2013; Michaelides et al., 2012). These results reveal that binge eating,
711 characterized by transients and sudden urges of hedonic drive, requires, at least in
712 its early phases, a D1R-mediated transmission. This D1R-dependent mechanism is
713 in line with the affinity and time-dependent dynamics of dopamine effects (Luo et al.,
714 2011) as well as with the molecular action of released DA which, by binding to

715 Ga(olf)-coupled D1R, would trigger the activation of the aforementioned pathways,
716 whether activation of the Gi-coupled D2R would lead to their inhibition (Beaulieu and
717 Gainetdinov, 2011; Valjent et al., 2019). However, in clear opposition to
718 psychostimulants, which directly act at central DA synapses, food and food-mediated
719 behaviors impact DA transmission through a plethora of indirect and often
720 peripherally born long-range acting mediators. In fact, the central regulation of
721 feeding behavior, either in its homeostatic and/or hedonic components, tightly
722 depends on the fine orchestration of peripheral humoral and neuronal signals.
723 Notably, nutrients, as demonstrated by intragastric infusion of fat and sugar (Alhadeff
724 et al., 2019; Han et al., 2016; Hankir et al., 2017; Tellez et al., 2016), or gut-born
725 signals (Cone et al., 2014; Fulton et al., 2006; Jerlhag et al., 2007; Reddy et al.,
726 2018), are sufficient to modulate DA release in reward-related structures. Here, we
727 observed that gut-born signals such as CCK, GLP1 and endocannabinoids (eCBs)
728 are essential in gating bingeing. In particular, we found that time-locked consumption
729 of palatable food was associated with a rise in peripheral endogenous eCBs, notably
730 2-AG. Furthermore, inhibition of the 2-AG-degrading enzyme MAG lipase resulted in
731 a potentiation of palatable food consumption. Thus, by taking advantage of a
732 peripherally restricted CB1R antagonist (Tam et al., 2010), we observed that
733 administration of AM6545 was able to fully abolish both anticipatory and
734 consummatory phases of hedonic feeding as well as the potentiated feeding induced
735 by the MAG lipase inhibitor. These effects agree with the literature showing that
736 endogenous peripheral eCBs are highly and dynamically modulated in eating
737 disorders, and act as powerful mediators of the gut-to-brain integration (Gómez et al.,
738 2002).

739

740 Previous studies have shown that chronic administration of AM6545 promoted
741 long-term maintenance of weight loss and reduction of dyslipidemia in obesity (Boon
742 et al., 2014; Cluny et al., 2010; Tam et al., 2010). Here, we show that single, as well
743 as repeated (4 days), administration of AM6545 potently inhibits binge eating without
744 altering body weight. The anorectic effects of peripheral blockade of CB1R have
745 been, at least in part, attributed to the property of CB1R antagonists to promote fatty
746 acid oxidation (FAO). In agreement with these studies, we have observed that acute
747 administration of AM6545 was able to dramatically increase FAO independently of
748 food intake. However, here we also demonstrate that such effects require the vagus

749 nerve since subdiaphragmatic vagotomy prevents both AM6545-mediated bingeing
750 blockade and FAO increase. The action of endogenous eCBs as well as of AM6545
751 on CB1R-expressing vagal afferents (Burdyga et al., 2010; Egerod et al., 2018) may
752 explain our results. In fact, an increase in endogenous eCBs during palatable
753 feeding, in virtue of the inhibitory Gi-coupled signaling of CB1R, would inhibit the
754 vagus nerve thus delaying NTS-reaching satiety signals and promoting food intake.
755 On the contrary, peripheral blockade of CB1R, especially when peripheral eCB levels
756 are endogenously high (i.e. binge eating, bulimia, obesity), would lead to a prompt
757 disinhibition and to the concomitant activation of satietogenic brain pathways
758 (NTS→PBN→PVN). Interestingly, it is worth to mention that in a non-hedonic feeding
759 paradigm the anorectic properties of AM6545 did not require the vagus nerve (Cluny
760 et al., 2010) and that under fasting or lipoprivic conditions the systemic CB1R inverse
761 agonist SR141716A (rimonabant) modulated feeding by the sympathetic nervous
762 system (SNS) (Bellocchio et al., 2013). Another site of action for peripheral eCBs is
763 represented by CB1R-expressing gut cells (Argueta et al., 2019; Godlewski et al.,
764 2019). Interestingly, oral administration of a peripheral CB1R antagonist resulted in a
765 reduction of alcohol intake via a ghrelin-dependent and vagus-mediated mechanism
766 (Godlewski et al., 2019). However, in our reward-driven feeding model, oral
767 administration of AM6545 failed in mediating its modifications on metabolic efficiency
768 as well as in preventing bingeing behavior, thus suggesting that lumen-oriented
769 apical CB1R may not be involved in our mechanism. Intriguingly, recent studies have
770 uncovered that sensory neuropod cells in the gut (Bohórquez et al., 2014, 2015) can
771 synaptically signal with the juxtaposed vagal afferents using, among other possible
772 mediators (Glass et al., 2017; Haber et al., 2017), the fast-acting neurotransmitter
773 glutamate (Kaelberer et al., 2018). Whether this specialized gut-to-nerve synapse
774 also mobilizes eCBs, as it occurs at most central excitatory synapses, remains to be
775 determined.

776 Overall, it would not be hazardous to suggest that peripheral eCBs may impact
777 feeding patterns through different integrative mechanisms which, depending on the
778 location of peripheral CB1R, may strongly modulate distinct functional outputs.
779 Indeed, these results call for a need to use cell-type and tissue-type-specific
780 strategies to selectively delete CB1R and/or eCBs-producing enzymes in distinct
781 compartments of the gastrointestinal tract and in the neuronal gut-brain axis.

782 In order to anatomically provide an explanatory gut-to-brain circuit able to support the
783 vagus-mediated action of AM6545, we found a stark increase of cFos, a marker of
784 neuronal activity, in key brain regions of the satietogenic neuronal pathway.
785 Importantly, we reveal that blockade of peripheral CB1R signaling resulted in a
786 strong vagus-dependent activation of the NTS as well as of its downstream
787 connected structures, notably the IPBN and the hypothalamic PVN. This segmented
788 activation of the gut→brainstem→hypothalamus path is most likely responsible for
789 the AM6545-induced effects on bingeing and energy homeostasis since structure-
790 specific activation of these nodes has been shown to reduce food intake and alter
791 energy homeostasis (An et al., 2020; Campos et al., 2016; Carter et al., 2013;
792 D'Agostino et al., 2016; Li et al., 2019a, 2019b; Roman et al., 2016). In addition to
793 this satietogenic path and given the strong reward component of our time-locked
794 feeding paradigm, we also uncover that AM6545-mediated vagus activation results in
795 a dampened activation of VTA DA-neurons. In fact, peripheral blockade of CB1R also
796 resulted in a stark blunting of the DA-dependent GBR-evoked increased locomotor
797 activity and DA-mediated cFos expression in the nucleus accumbens, a functional
798 output that requires the intact vagal gut-brain axis. However, such effect did not
799 depend on the releasing capabilities of DA neurons since AM6545 failed in altering
800 amphetamine-evoked locomotor activity. In addition, taking advantage of virally
801 mediated GCaMP6f-evoked *in vivo* Ca²⁺ imaging of putative VTA DA-neurons
802 (Anzalone et al., 2012; Bello et al., 2011), here we demonstrate that peripheral
803 blockade of CB1R clearly reduces both basal and evoked activity of DA-neurons, a
804 feature resembling the effects of vagal nerve stimulation (Manta et al., 2013; Perez et
805 al., 2014).

806 The VTA has a heterogeneous connectivity (Morales and Margolis, 2017) and a
807 single and monosynaptic circuit responsible for the inhibition DA-neurons through the
808 AM6545-activated vagus nerve cannot be selectively sorted out yet. However,
809 several satiety-related structures in the brainstem, hindbrain and hypothalamus are
810 known to project and modulate, directly or indirectly, VTA DA-neurons (Alhadeff et
811 al., 2012; Boughter et al., 2019; Faget et al., 2016; Grill and Hayes, 2012; Han et al.,
812 2018; Nieh et al., 2016; Wang et al., 2015). Among these circuits, the PBN→VTA
813 relay is of particular interest since excitatory PBN neurons also largely contact VTA
814 GABA-neurons (Beier et al., 2015; Faget et al., 2016) which in turn may drive the

815 inhibition of VTA DA-neurons and consequent dampening of motivated
816 behaviors.

817

818 Here, we show that DA-dependent adaptations require orchestrated inputs
819 among which peripheral endocannabinoids, through the vagus nerve, allostatically
820 scale the homeostatic and hedonic components of feeding and act as mandatory
821 gatekeepers for adaptive responses of the reward circuit. Indeed, the gut-brain axis is
822 increasingly incriminated as a key player of the regulation of energy metabolism
823 (Clemmensen et al., 2017), and we show for the first time that BE is under the control
824 of the vagus-mediated peripheral inputs. Pointing the peripheral eCBs as permissive
825 actors of this eating disorder certainly brings novelty in the clinical investigations
826 aimed at identifying innovative and non-invasive therapeutic strategies. Importantly,
827 this study further points the gut-brain axis as privileged target to modulate brain
828 structures that are functionally responsible for processing integrative cognitive and
829 reward.

830 In conclusion, while further studies are warrant to fully untangle the key enteric actors
831 responsible for this phenomenon, our study identifies a novel integrative mechanism
832 by which peripheral endocannabinoids through the vagal gut-brain axis gate allostatic
833 feeding by controlling satiety and reward events, thus also paving the way to target
834 peripheral elements for brain disorders.

835 **Acknowledgments**

836 We thank Chloé Morel, Rim Hassouna, Anne-Sophie Delbes, Daniela Herrera Moro
837 and Raphaël Denis for technical advice and support. Adrien Paquot
838 (BPBL/UCLouvain) is acknowledged for its help with eCB quantification. We thank
839 Olja Kacanski for administrative support, Isabelle Le Parco, Ludovic Maingault,
840 Angélique Dauvin, Aurélie Djemat, Florianne Michel, Magguy Boa and Daniel
841 Quintas for animals' care and Sabria Allithi for genotyping. We acknowledge the
842 technical platform Functional and Physiological Exploration platform (FPE) of the
843 Université de Paris (BFA - UMR 8251) and the animal core facility Buffon of the
844 Université de Paris/Institut Jacques Monod. This work was supported by the Fyssen
845 Foundation, Nutricia Research Foundation, Allen Foundation Inc., Université de Paris
846 and CNRS. CB and EM were supported by fellowships from the *Fondation pour la*
847 *Recherche Médicale* (FRM).

848

849 **Author Contributions**

850 C.B. and G.G. conceived, designed, performed and analyzed most of the
851 experiments. J.C. performed surgeries and behavioral experiments. E.M. helped with
852 molecular studies. E.F. performed vagotomy. C.M. helped with fiber photometry
853 experiments. G.G.M. analyzed endocannabinoids levels. S.L. provided scientific
854 guidance and critical feedback. S.L. and G.G. secured funding. G.G. supervised the
855 whole project, interpreted the data and wrote the manuscript with contribution from all
856 coauthors.

857

858 **Declaration of Interests**

859 The authors declare no competing interests.

860 References

- 861 Alhadeff, A.L., Rupprecht, L.E., and Hayes, M.R. (2012). GLP-1 neurons in the
862 nucleus of the solitary tract project directly to the ventral tegmental area and nucleus
863 accumbens to control for food intake. *Endocrinology* 153, 647–658.
- 864 Alhadeff, A.L., Goldstein, N., Park, O., Klima, M.L., Vargas, A., and Betley, J.N.
865 (2019). Natural and Drug Rewards Engage Distinct Pathways that Converge on
866 Coordinated Hypothalamic and Reward Circuits. *Neuron* 103, 891-908.e6.
- 867 An, J.J., Kinney, C.E., Tan, J.-W., Liao, G.-Y., Kremer, E.J., and Xu, B. (2020). TrkB-
868 expressing paraventricular hypothalamic neurons suppress appetite through multiple
869 neurocircuits. *Nat Commun* 11, 1729.
- 870 Anzalone, A., Lizardi-Ortiz, J.E., Ramos, M., De Mei, C., Hopf, F.W., Iaccarino, C.,
871 Halbout, B., Jacobsen, J., Kinoshita, C., Welter, M., et al. (2012). Dual control of
872 dopamine synthesis and release by presynaptic and postsynaptic dopamine D2
873 receptors. *J Neurosci* 32, 9023–9034.
- 874 de Araujo, I.E., Schatzker, M., and Small, D.M. (2020). Rethinking Food Reward.
875 *Annual Review of Psychology* 71, 139–164.
- 876 Arch, J.R.S., Hislop, D., Wang, S.J.Y., and Speakman, J.R. (2006). Some
877 mathematical and technical issues in the measurement and interpretation of open-
878 circuit indirect calorimetry in small animals. *Int J Obes (Lond)* 30, 1322–1331.
- 879 Argueta, D.A., and DiPatrizio, N.V. (2017). Peripheral endocannabinoid signaling
880 controls hyperphagia in western diet-induced obesity. *Physiol Behav* 171, 32–39.
- 881 Argueta, D.A., Perez, P.A., Makriyannis, A., and DiPatrizio, N.V. (2019). Cannabinoid
882 CB1 Receptors Inhibit Gut-Brain Satiating Signaling in Diet-Induced Obesity. *Front*
883 *Physiol* 10, 704.
- 884 Avena, N.M. (2010). The study of food addiction using animal models of binge eating.
885 *Appetite* 55, 734–737.
- 886 Bai, L., Mesgarzadeh, S., Ramesh, K.S., Huey, E.L., Liu, Y., Gray, L.A., Aitken, T.J.,
887 Chen, Y., Beutler, L.R., Ahn, J.S., et al. (2019). Genetic Identification of Vagal
888 Sensory Neurons That Control Feeding. *Cell* 179, 1129-1143.e23.
- 889 Bake, T., Murphy, M., Morgan, D.G.A., and Mercer, J.G. (2014). Large, binge-type
890 meals of high fat diet change feeding behaviour and entrain food anticipatory activity
891 in mice. *Appetite* 77, 60–71.
- 892 Balodis, I.M., Grilo, C.M., and Potenza, M.N. (2015). Neurobiological features of
893 binge eating disorder. *CNS Spectr* 20, 557–565.
- 894 Beaulieu, J.-M., and Gainetdinov, R.R. (2011). The physiology, signaling, and
895 pharmacology of dopamine receptors. *Pharmacol. Rev.* 63, 182–217.
- 896 Beier, K.T., Steinberg, E.E., DeLoach, K.E., Xie, S., Miyamichi, K., Schwarz, L., Gao,
897 X.J., Kremer, E.J., Malenka, R.C., and Luo, L. (2015). Circuit Architecture of VTA
898 Dopamine Neurons Revealed by Systematic Input-Output Mapping. *Cell* 162, 622–
899 634.
- 900 Bello, E.P., Mateo, Y., Gelman, D.M., Noaín, D., Shin, J.H., Low, M.J., Alvarez, V.A.,
901 Lovinger, D.M., and Rubinstein, M. (2011). Cocaine supersensitivity and enhanced
902 motivation for reward in mice lacking dopamine D2 autoreceptors. *Nat Neurosci* 14,
903 1033–1038.
- 904 Bellocchio, L., Soria-Gómez, E., Quarta, C., Metna-Laurent, M., Cardinal, P., Binder,
905 E., Cannich, A., Delamarre, A., Häring, M., Martín-Fontecha, M., et al. (2013).
906 Activation of the sympathetic nervous system mediates hypophagic and anxiety-like
907 effects of CB₁ receptor blockade. *Proc Natl Acad Sci U S A* 110, 4786–4791.
- 908 Berthoud, H.-R., Münzberg, H., and Morrison, C.D. (2017). Blaming the Brain for
909 Obesity: Integration of Hedonic and Homeostatic Mechanisms. *Gastroenterology*

910 152, 1728–1738.

911 Bertran-Gonzalez, J., Bosch, C., Maroteaux, M., Matamales, M., Hervé, D., Valjent,
912 E., and Girault, J.-A. (2008). Opposing patterns of signaling activation in dopamine
913 D1 and D2 receptor-expressing striatal neurons in response to cocaine and
914 haloperidol. *J. Neurosci.* 28, 5671–5685.

915 Beutler, L.R., Corpuz, T.V., Ahn, J.S., Kosar, S., Song, W., Chen, Y., and Knight,
916 Z.A. (2020). Obesity causes selective and long-lasting desensitization of AgRP
917 neurons to dietary fat. *Elife* 9.

918 Biever, A., Puighermanal, E., Nishi, A., David, A., Panciatici, C., Longueville, S.,
919 Xirodimas, D., Gangarossa, G., Meyuhas, O., Hervé, D., et al. (2015). PKA-
920 dependent phosphorylation of ribosomal protein S6 does not correlate with
921 translation efficiency in striatonigral and striatopallidal medium-sized spiny neurons.
922 *J. Neurosci.* 35, 4113–4130.

923 Bohórquez, D.V., Samsa, L.A., Roholt, A., Medicetty, S., Chandra, R., and Liddle,
924 R.A. (2014). An enteroendocrine cell-enteric glia connection revealed by 3D electron
925 microscopy. *PLoS One* 9, e89881.

926 Bohórquez, D.V., Shahid, R.A., Erdmann, A., Kreger, A.M., Wang, Y., Calakos, N.,
927 Wang, F., and Liddle, R.A. (2015). Neuroepithelial circuit formed by innervation of
928 sensory enteroendocrine cells. *J Clin Invest* 125, 782–786.

929 Boon, M.R., Kooijman, S., van Dam, A.D., Pelgrom, L.R., Berbée, J.F.P., Visseren,
930 C.A.R., van Aggele, R.C., van den Hoek, A.M., Sips, H.C.M., Lombès, M., et al.
931 (2014). Peripheral cannabinoid 1 receptor blockade activates brown adipose tissue
932 and diminishes dyslipidemia and obesity. *FASEB J* 28, 5361–5375.

933 Botteman, P., Paquot, A., Ameraoui, H., Alhouayek, M., and Muccioli, G.G. (2019).
934 The α/β -hydrolase domain 6 inhibitor WWL70 decreases endotoxin-induced lung
935 inflammation in mice, potential contribution of 2-arachidonoylglycerol, and
936 lysoglycerophospholipids. *FASEB J* 33, 7635–7646.

937 Boughter, J.D., Lu, L., Saites, L.N., and Tokita, K. (2019). Sweet and bitter taste
938 stimuli activate VTA projection neurons in the parabrachial nucleus. *Brain Res* 1714,
939 99–110.

940 Burdyga, G., Varro, A., Dimaline, R., Thompson, D.G., and Dockray, G.J. (2010).
941 Expression of cannabinoid CB1 receptors by vagal afferent neurons: kinetics and role
942 in influencing neurochemical phenotype. *Am J Physiol Gastrointest Liver Physiol* 299,
943 G63-69.

944 Campos, C.A., Bowen, A.J., Schwartz, M.W., and Palmiter, R.D. (2016). Parabrachial
945 CGRP Neurons Control Meal Termination. *Cell Metab* 23, 811–820.

946 Capasso, A., Milano, W., and Cauli, O. (2018). Changes in the Peripheral
947 Endocannabinoid System as a Risk Factor for the Development of Eating Disorders.
948 *Endocr Metab Immune Disord Drug Targets* 18, 325–332.

949 Caravaggio, F., Raitsin, S., Gerretsen, P., Nakajima, S., Wilson, A., and Graff-
950 Guerrero, A. (2015). Ventral striatum binding of a dopamine D2/3 receptor agonist
951 but not antagonist predicts normal body mass index. *Biol Psychiatry* 77, 196–202.

952 Carr, M.M., and Grilo, C.M. (2020). Examining heterogeneity of binge-eating disorder
953 using latent class analysis. *J Psychiatr Res* 130, 194–200.

954 Carter, M.E., Soden, M.E., Zweifel, L.S., and Palmiter, R.D. (2013). Genetic
955 identification of a neural circuit that suppresses appetite. *Nature* 503, 111–114.

956 Cheng, W., Gonzalez, I., Pan, W., Tsang, A.H., Adams, J., Ndoka, E., Gordian, D.,
957 Khoury, B., Roelofs, K., Evers, S.S., et al. (2020). Calcitonin Receptor Neurons in the
958 Mouse Nucleus Tractus Solitarius Control Energy Balance via the Non-aversive
959 Suppression of Feeding. *Cell Metab* 31, 301-312.e5.

- 960 Clemmensen, C., Müller, T.D., Woods, S.C., Berthoud, H.-R., Seeley, R.J., and
961 Tschöp, M.H. (2017). Gut-Brain Cross-Talk in Metabolic Control. *Cell* *168*, 758–774.
- 962 Cluny, N.L., Vemuri, V.K., Chambers, A.P., Limebeer, C.L., Bedard, H., Wood, J.T.,
963 Lutz, B., Zimmer, A., Parker, L.A., Makriyannis, A., et al. (2010). A novel peripherally
964 restricted cannabinoid receptor antagonist, AM6545, reduces food intake and body
965 weight, but does not cause malaise, in rodents. *Br J Pharmacol* *161*, 629–642.
- 966 Coll, A.P., Farooqi, I.S., and O’Rahilly, S. (2007). The hormonal control of food
967 intake. *Cell* *129*, 251–262.
- 968 Cone, J.J., McCutcheon, J.E., and Roitman, M.F. (2014). Ghrelin acts as an interface
969 between physiological state and phasic dopamine signaling. *J Neurosci* *34*, 4905–
970 4913.
- 971 D’Agostino, G., Lyons, D.J., Cristiano, C., Burke, L.K., Madara, J.C., Campbell, J.N.,
972 Garcia, A.P., Land, B.B., Lowell, B.B., Dileone, R.J., et al. (2016). Appetite controlled
973 by a cholecystikinin nucleus of the solitary tract to hypothalamus neurocircuit. *Elife*
974 *5*.
- 975 De Ridder, D., Manning, P., Leong, S.L., Ross, S., and Vanneste, S. (2016).
976 Allostatics in health and food addiction. *Sci Rep* *6*, 37126.
- 977 DiFeliceantonio, A.G., Coppin, G., Rigoux, L., Edwin Thanarajah, S., Dagher, A.,
978 Tittgemeyer, M., and Small, D.M. (2018). Supra-Additive Effects of Combining Fat
979 and Carbohydrate on Food Reward. *Cell Metab* *28*, 33-44.e3.
- 980 DiPatrizio, N.V., and Piomelli, D. (2015). Intestinal lipid-derived signals that sense
981 dietary fat. *J Clin Invest* *125*, 891–898.
- 982 DiPatrizio, N.V., Joslin, A., Jung, K.-M., and Piomelli, D. (2013). Endocannabinoid
983 signaling in the gut mediates preference for dietary unsaturated fats. *FASEB J* *27*,
984 2513–2520.
- 985 Egerod, K.L., Petersen, N., Timshel, P.N., Rekling, J.C., Wang, Y., Liu, Q., Schwartz,
986 T.W., and Gautron, L. (2018). Profiling of G protein-coupled receptors in vagal
987 afferents reveals novel gut-to-brain sensing mechanisms. *Mol Metab* *12*, 62–75.
- 988 Even, P.C., and Nadkarni, N.A. (2012). Indirect calorimetry in laboratory mice and
989 rats: principles, practical considerations, interpretation and perspectives. *Am J*
990 *Physiol Regul Integr Comp Physiol* *303*, R459-476.
- 991 Faget, L., Osakada, F., Duan, J., Ressler, R., Johnson, A.B., Proudfoot, J.A., Yoo,
992 J.H., Callaway, E.M., and Hnasko, T.S. (2016). Afferent Inputs to Neurotransmitter-
993 Defined Cell Types in the Ventral Tegmental Area. *Cell Rep* *15*, 2796–2808.
- 994 Fernandes, A.B., Alves da Silva, J., Almeida, J., Cui, G., Gerfen, C.R., Costa, R.M.,
995 and Oliveira-Maia, A.J. (2020). Postingestive Modulation of Food Seeking Depends
996 on Vagus-Mediated Dopamine Neuron Activity. *Neuron* *106*, 778-788.e6.
- 997 Fulton, S., Pissios, P., Manchon, R.P., Stiles, L., Frank, L., Pothos, E.N., Maratos-
998 Flier, E., and Flier, J.S. (2006). Leptin regulation of the mesoaccumbens dopamine
999 pathway. *Neuron* *51*, 811–822.
- 1000 Gangarossa, G., Perroy, J., and Valjent, E. (2013a). Combinatorial topography and
1001 cell-type specific regulation of the ERK pathway by dopaminergic agonists in the
1002 mouse striatum. *Brain Struct Funct* *218*, 405–419.
- 1003 Gangarossa, G., Espallergues, J., de Kerchove d’Exaerde, A., El Mestikawy, S.,
1004 Gerfen, C.R., Hervé, D., Girault, J.-A., and Valjent, E. (2013b). Distribution and
1005 compartmental organization of GABAergic medium-sized spiny neurons in the mouse
1006 nucleus accumbens. *Front Neural Circuits* *7*, 22.
- 1007 Gangarossa, G., Castell, L., Castro, L., Tarot, P., Veyrunes, F., Vincent, P., Bertaso,
1008 F., and Valjent, E. (2019). Contrasting patterns of ERK activation in the tail of the
1009 striatum in response to aversive and rewarding signals. *J. Neurochem.* *151*, 204–

1010 226.
1011 George, O., Le Moal, M., and Koob, G.F. (2012). Allostasis and addiction: role of the
1012 dopamine and corticotropin-releasing factor systems. *Physiol Behav* 106, 58–64.
1013 Glass, L.L., Calero-Nieto, F.J., Jawaid, W., Larraufie, P., Kay, R.G., Göttgens, B.,
1014 Reimann, F., and Gribble, F.M. (2017). Single-cell RNA-sequencing reveals a distinct
1015 population of proglucagon-expressing cells specific to the mouse upper small
1016 intestine. *Mol Metab* 6, 1296–1303.
1017 Godlewski, G., Cinar, R., Coffey, N.J., Liu, J., Jourdan, T., Mukhopadhyay, B.,
1018 Chedester, L., Liu, Z., Osei-Hyiaman, D., Iyer, M.R., et al. (2019). Targeting
1019 Peripheral CB1 Receptors Reduces Ethanol Intake via a Gut-Brain Axis. *Cell Metab*
1020 29, 1320-1333.e8.
1021 Gómez, R., Navarro, M., Ferrer, B., Trigo, J.M., Bilbao, A., Del Arco, I., Cippitelli, A.,
1022 Nava, F., Piomelli, D., and Rodríguez de Fonseca, F. (2002). A peripheral
1023 mechanism for CB1 cannabinoid receptor-dependent modulation of feeding. *J*
1024 *Neurosci* 22, 9612–9617.
1025 Gore, B.B., and Zweifel, L.S. (2013). Genetic reconstruction of dopamine D1 receptor
1026 signaling in the nucleus accumbens facilitates natural and drug reward responses. *J*
1027 *Neurosci* 33, 8640–8649.
1028 Gribble, F.M., and Reimann, F. (2019). Function and mechanisms of enteroendocrine
1029 cells and gut hormones in metabolism. *Nat Rev Endocrinol* 15, 226–237.
1030 Grill, H.J., and Hayes, M.R. (2012). Hindbrain neurons as an essential hub in the
1031 neuroanatomically distributed control of energy balance. *Cell Metab* 16, 296–309.
1032 Haber, A.L., Biton, M., Rogel, N., Herbst, R.H., Shekhar, K., Smillie, C., Burgin, G.,
1033 Delorey, T.M., Howitt, M.R., Katz, Y., et al. (2017). A single-cell survey of the small
1034 intestinal epithelium. *Nature* 551, 333–339.
1035 Han, W., Tellez, L.A., Niu, J., Medina, S., Ferreira, T.L., Zhang, X., Su, J., Tong, J.,
1036 Schwartz, G.J., van den Pol, A., et al. (2016). Striatal Dopamine Links
1037 Gastrointestinal Rerouting to Altered Sweet Appetite. *Cell Metab* 23, 103–112.
1038 Han, W., Tellez, L.A., Perkins, M.H., Perez, I.O., Qu, T., Ferreira, J., Ferreira, T.L.,
1039 Quinn, D., Liu, Z.-W., Gao, X.-B., et al. (2018). A Neural Circuit for Gut-Induced
1040 Reward. *Cell* 175, 665-678.e23.
1041 Hankir, M.K., Seyfried, F., Hintschich, C.A., Diep, T.-A., Kleberg, K., Kranz, M.,
1042 Deuther-Conrad, W., Tellez, L.A., Rullmann, M., Patt, M., et al. (2017). Gastric
1043 Bypass Surgery Recruits a Gut PPAR- α -Striatal D1R Pathway to Reduce Fat
1044 Appetite in Obese Rats. *Cell Metab.* 25, 335–344.
1045 Hutson, P.H., Balodis, I.M., and Potenza, M.N. (2018). Binge-eating disorder: Clinical
1046 and therapeutic advances. *Pharmacol Ther* 182, 15–27.
1047 Izzo, A.A., Piscitelli, F., Capasso, R., Aviello, G., Romano, B., Borrelli, F., Petrosino,
1048 S., and Di Marzo, V. (2009). Peripheral endocannabinoid dysregulation in obesity:
1049 relation to intestinal motility and energy processing induced by food deprivation and
1050 re-feeding. *Br J Pharmacol* 158, 451–461.
1051 Jerlhag, E., Egecioglu, E., Dickson, S.L., Douhan, A., Svensson, L., and Engel, J.A.
1052 (2007). Ghrelin administration into tegmental areas stimulates locomotor activity and
1053 increases extracellular concentration of dopamine in the nucleus accumbens. *Addict*
1054 *Biol* 12, 6–16.
1055 Kaelberer, M.M., Buchanan, K.L., Klein, M.E., Barth, B.B., Montoya, M.M., Shen, X.,
1056 and Bohórquez, D.V. (2018). A gut-brain neural circuit for nutrient sensory
1057 transduction. *Science* 361.
1058 Kai, N., Nishizawa, K., Tsutsui, Y., Ueda, S., and Kobayashi, K. (2015). Differential
1059 roles of dopamine D1 and D2 receptor-containing neurons of the nucleus accumbens

1060 shell in behavioral sensitization. *J Neurochem* 135, 1232–1241.

1061 Kenny, P.J., Voren, G., and Johnson, P.M. (2013). Dopamine D2 receptors and
1062 striatopallidal transmission in addiction and obesity. *Curr Opin Neurobiol* 23, 535–
1063 538.

1064 Keramati, M., and Gutkin, B. (2014). Homeostatic reinforcement learning for
1065 integrating reward collection and physiological stability. *Elife* 3.

1066 Kobayashi, T., Araki, T., Itoyama, Y., Takeshita, M., Ohta, T., and Oshima, Y. (1997).
1067 Effects of L-dopa and bromocriptine on haloperidol-induced motor deficits in mice.
1068 *Life Sci* 61, 2529–2538.

1069 Kolata, S.M., Nakao, K., Jeevakumar, V., Farmer-Alroth, E.L., Fujita, Y., Bartley,
1070 A.F., Jiang, S.Z., Rompala, G.R., Sorge, R.E., Jimenez, D.V., et al. (2018).
1071 Neuropsychiatric Phenotypes Produced by GABA Reduction in Mouse Cortex and
1072 Hippocampus. *Neuropsychopharmacology* 43, 1445–1456.

1073 Kuipers, E.N., Kantae, V., Maarse, B.C.E., van den Berg, S.M., van Eenige, R.,
1074 Nahon, K.J., Reifel-Miller, A., Coskun, T., de Winther, M.P.J., Lutgens, E., et al.
1075 (2018). High Fat Diet Increases Circulating Endocannabinoids Accompanied by
1076 Increased Synthesis Enzymes in Adipose Tissue. *Front Physiol* 9, 1913.

1077 Ladenheim, E.E. (2015). Liraglutide and obesity: a review of the data so far. *Drug*
1078 *Des Devel Ther* 9, 1867–1875.

1079 de Lartigue, G. (2016). Role of the vagus nerve in the development and treatment of
1080 diet-induced obesity. *J Physiol* 594, 5791–5815.

1081 Lau, B.K., Cota, D., Cristino, L., and Borgland, S.L. (2017). Endocannabinoid
1082 modulation of homeostatic and non-homeostatic feeding circuits.
1083 *Neuropharmacology* 124, 38–51.

1084 Lenard, N.R., and Berthoud, H.-R. (2008). Central and peripheral regulation of food
1085 intake and physical activity: pathways and genes. *Obesity (Silver Spring)* 16 *Suppl* 3,
1086 S11-22.

1087 Lerner, T.N., Shilyansky, C., Davidson, T.J., Evans, K.E., Beier, K.T., Zalocusky,
1088 K.A., Crow, A.K., Malenka, R.C., Luo, L., Tomer, R., et al. (2015). Intact-Brain
1089 Analyses Reveal Distinct Information Carried by SNc Dopamine Subcircuits. *Cell*
1090 162, 635–647.

1091 Li, C., Navarrete, J., Liang-Guallpa, J., Lu, C., Funderburk, S.C., Chang, R.B.,
1092 Liberles, S.D., Olson, D.P., and Krashes, M.J. (2019a). Defined Paraventricular
1093 Hypothalamic Populations Exhibit Differential Responses to Food Contingent on
1094 Caloric State. *Cell Metab* 29, 681-694.e5.

1095 Li, M.M., Madara, J.C., Steger, J.S., Krashes, M.J., Balthasar, N., Campbell, J.N.,
1096 Resch, J.M., Conley, N.J., Garfield, A.S., and Lowell, B.B. (2019b). The
1097 Paraventricular Hypothalamus Regulates Satiety and Prevents Obesity via Two
1098 Genetically Distinct Circuits. *Neuron* 102, 653-667.e6.

1099 Linehan, V., Fang, L.Z., Parsons, M.P., and Hirasawa, M. (2020). High-fat diet
1100 induces time-dependent synaptic plasticity of the lateral hypothalamus. *Mol Metab*
1101 36, 100977.

1102 Long, J.Z., Li, W., Booker, L., Burston, J.J., Kinsey, S.G., Schlosburg, J.E., Pavón,
1103 F.J., Serrano, A.M., Selley, D.E., Parsons, L.H., et al. (2009). Selective blockade of
1104 2-arachidonoylglycerol hydrolysis produces cannabinoid behavioral effects. *Nat*
1105 *Chem Biol* 5, 37–44.

1106 Luo, Z., Volkow, N.D., Heintz, N., Pan, Y., and Du, C. (2011). Acute cocaine induces
1107 fast activation of D1 receptor and progressive deactivation of D2 receptor striatal
1108 neurons: in vivo optical microprobe [Ca²⁺]_i imaging. *J Neurosci* 31, 13180–13190.

1109 Lutter, M., and Nestler, E.J. (2009). Homeostatic and hedonic signals interact in the

1110 regulation of food intake. *J Nutr* 139, 629–632.

1111 Malbert, C.-H., Genissel, M., Divoux, J.-L., and Henry, C. (2019). Chronic abdominal
1112 vagus stimulation increased brain metabolic connectivity, reduced striatal dopamine
1113 transporter and increased mid-brain serotonin transporter in obese miniature pigs. *J*
1114 *Transl Med* 17, 78.

1115 Manta, S., El Mansari, M., Debonnel, G., and Blier, P. (2013). Electrophysiological
1116 and neurochemical effects of long-term vagus nerve stimulation on the rat
1117 monoaminergic systems. *Int J Neuropsychopharmacol* 16, 459–470.

1118 Mazier, W., Saucisse, N., Simon, V., Cannich, A., Marsicano, G., Massa, F., and
1119 Cota, D. (2019). mTORC1 and CB1 receptor signaling regulate excitatory
1120 glutamatergic inputs onto the hypothalamic paraventricular nucleus in response to
1121 energy availability. *Mol Metab* 28, 151–159.

1122 McEwen, B.S., and Wingfield, J.C. (2003). The concept of allostasis in biology and
1123 biomedicine. *Horm Behav* 43, 2–15.

1124 Michaelides, M., Thanos, P.K., Kim, R., Cho, J., Ananth, M., Wang, G.-J., and
1125 Volkow, N.D. (2012). PET imaging predicts future body weight and cocaine
1126 preference. *Neuroimage* 59, 1508–1513.

1127 Monteleone, A.M., Di Marzo, V., Monteleone, P., Dalle Grave, R., Aveta, T., Ghoch,
1128 M.E., Piscitelli, F., Volpe, U., Calugi, S., and Maj, M. (2016). Responses of peripheral
1129 endocannabinoids and endocannabinoid-related compounds to hedonic eating in
1130 obesity. *Eur J Nutr* 55, 1799–1805.

1131 Monteleone, A.M., Piscitelli, F., Dalle Grave, R., El Ghoch, M., Di Marzo, V., Maj, M.,
1132 and Monteleone, P. (2017). Peripheral Endocannabinoid Responses to Hedonic
1133 Eating in Binge-Eating Disorder. *Nutrients* 9.

1134 Monteleone, P., Matias, I., Martiadis, V., De Petrocellis, L., Maj, M., and Di Marzo, V.
1135 (2005). Blood levels of the endocannabinoid anandamide are increased in anorexia
1136 nervosa and in binge-eating disorder, but not in bulimia nervosa.
1137 *Neuropsychopharmacology* 30, 1216–1221.

1138 Morales, M., and Margolis, E.B. (2017). Ventral tegmental area: cellular
1139 heterogeneity, connectivity and behaviour. *Nat Rev Neurosci* 18, 73–85.

1140 Muñoz-Escobar, G., Guerrero-Vargas, N.N., and Escobar, C. (2019). Random
1141 access to palatable food stimulates similar addiction-like responses as a fixed
1142 schedule, but only a fixed schedule elicits anticipatory activation. *Sci Rep* 9, 18223.

1143 Naish, K.R., Laliberte, M., MacKillop, J., and Balodis, I.M. (2019). Systematic review
1144 of the effects of acute stress in binge eating disorder. *Eur J Neurosci* 50, 2415–2429.

1145 Nieh, E.H., Vander Weele, C.M., Matthews, G.A., Presbrey, K.N., Wichmann, R.,
1146 Leppla, C.A., Izadmehr, E.M., and Tye, K.M. (2016). Inhibitory Input from the Lateral
1147 Hypothalamus to the Ventral Tegmental Area Disinhibits Dopamine Neurons and
1148 Promotes Behavioral Activation. *Neuron* 90, 1286–1298.

1149 Oosterman, J.E., Koekkoek, L.L., Foppen, E., Unmehopa, U.A., Eggels, L., Verheij,
1150 J., Fliers, E., la Fleur, S.E., and Kalsbeek, A. (2020). Synergistic Effect of Feeding
1151 Time and Diet on Hepatic Steatosis and Gene Expression in Male Wistar Rats.
1152 *Obesity (Silver Spring)* 28 Suppl 1, S81–S92.

1153 Palmiter, R.D. (2007). Is dopamine a physiologically relevant mediator of feeding
1154 behavior? *Trends Neurosci* 30, 375–381.

1155 Perez, S.M., Carreno, F.R., Frazer, A., and Lodge, D.J. (2014). Vagal nerve
1156 stimulation reverses aberrant dopamine system function in the methylazoxymethanol
1157 acetate rodent model of schizophrenia. *J Neurosci* 34, 9261–9267.

1158 Quarta, C., Mazza, R., Obici, S., Pasquali, R., and Pagotto, U. (2011). Energy
1159 balance regulation by endocannabinoids at central and peripheral levels. *Trends Mol*

- 1160 Med 17, 518–526.
- 1161 Rada, P., Avena, N.M., and Hoebel, B.G. (2005). Daily bingeing on sugar repeatedly
1162 releases dopamine in the accumbens shell. *Neuroscience* 134, 737–744.
- 1163 Radl, D., Chiacchiarretta, M., Lewis, R.G., Brami-Cherrier, K., Arcuri, L., and Borrelli,
1164 E. (2018). Differential regulation of striatal motor behavior and related cellular
1165 responses by dopamine D2L and D2S isoforms. *Proc Natl Acad Sci U S A* 115, 198–
1166 203.
- 1167 Ramsay, D.S., and Woods, S.C. (2014). Clarifying the roles of homeostasis and
1168 allostasis in physiological regulation. *Psychol Rev* 121, 225–247.
- 1169 Reddy, I.A., Smith, N.K., Erreger, K., Ghose, D., Saunders, C., Foster, D.J., Turner,
1170 B., Poe, A., Albaugh, V.L., McGuinness, O., et al. (2018). Bile diversion, a bariatric
1171 surgery, and bile acid signaling reduce central cocaine reward. *PLoS Biol* 16,
1172 e2006682.
- 1173 Reichelt, A.C., Westbrook, R.F., and Morris, M.J. (2015). Integration of reward
1174 signalling and appetite regulating peptide systems in the control of food-cue
1175 responses. *Br J Pharmacol* 172, 5225–5238.
- 1176 Roman, C.W., Derkach, V.A., and Palmiter, R.D. (2016). Genetically and functionally
1177 defined NTS to PBN brain circuits mediating anorexia. *Nat Commun* 7, 11905.
- 1178 Rossi, M.A., and Stuber, G.D. (2018). Overlapping Brain Circuits for Homeostatic and
1179 Hedonic Feeding. *Cell Metab.* 27, 42–56.
- 1180 Rossi, M.A., Basiri, M.L., McHenry, J.A., Kosyk, O., Otis, J.M., van den Munkhof,
1181 H.E., Bryois, J., Hübel, C., Breen, G., Guo, W., et al. (2019). Obesity remodels
1182 activity and transcriptional state of a lateral hypothalamic brake on feeding. *Science*
1183 364, 1271–1274.
- 1184 Saper, C.B., Chou, T.C., and Elmquist, J.K. (2002). The need to feed: homeostatic
1185 and hedonic control of eating. *Neuron* 36, 199–211.
- 1186 Small, D.M., Jones-Gotman, M., and Dagher, A. (2003). Feeding-induced dopamine
1187 release in dorsal striatum correlates with meal pleasantness ratings in healthy human
1188 volunteers. *Neuroimage* 19, 1709–1715.
- 1189 Spierling, S., de Guglielmo, G., Kirson, D., Kreisler, A., Roberto, M., George, O., and
1190 Zorrilla, E.P. (2020). Insula to ventral striatal projections mediate compulsive eating
1191 produced by intermittent access to palatable food. *Neuropsychopharmacology* 45,
1192 579–588.
- 1193 Sutton, L.P., and Caron, M.G. (2015). Essential role of D1R in the regulation of
1194 mTOR complex1 signaling induced by cocaine. *Neuropharmacology* 99, 610–619.
- 1195 Sykaras, A.G., Demenis, C., Case, R.M., McLaughlin, J.T., and Smith, C.P. (2012).
1196 Duodenal enteroendocrine I-cells contain mRNA transcripts encoding key
1197 endocannabinoid and fatty acid receptors. *PLoS One* 7, e42373.
- 1198 Takeuchi, T., Duszkiwicz, A.J., Sonneborn, A., Spooner, P.A., Yamasaki, M.,
1199 Watanabe, M., Smith, C.C., Fernández, G., Deisseroth, K., Greene, R.W., et al.
1200 (2016). Locus coeruleus and dopaminergic consolidation of everyday memory.
1201 *Nature* 537, 357–362.
- 1202 Tam, J., Vemuri, V.K., Liu, J., Bátkai, S., Mukhopadhyay, B., Godlewski, G., Osei-
1203 Hyiaman, D., Ohnuma, S., Ambudkar, S.V., Pickel, J., et al. (2010). Peripheral CB1
1204 cannabinoid receptor blockade improves cardiometabolic risk in mouse models of
1205 obesity. *J Clin Invest* 120, 2953–2966.
- 1206 Tellez, L.A., Medina, S., Han, W., Ferreira, J.G., Licon-Limón, P., Ren, X., Lam,
1207 T.T., Schwartz, G.J., and de Araujo, I.E. (2013). A gut lipid messenger links excess
1208 dietary fat to dopamine deficiency. *Science* 341, 800–802.
- 1209 Tellez, L.A., Han, W., Zhang, X., Ferreira, T.L., Perez, I.O., Shammah-Lagnado, S.J.,

- 1210 van den Pol, A.N., and de Araujo, I.E. (2016). Separate circuitries encode the
1211 hedonic and nutritional values of sugar. *Nat Neurosci* 19, 465–470.
- 1212 Usiello, A., Baik, J.H., Rougé-Pont, F., Picetti, R., Dierich, A., LeMeur, M., Piazza,
1213 P.V., and Borrelli, E. (2000). Distinct functions of the two isoforms of dopamine D2
1214 receptors. *Nature* 408, 199–203.
- 1215 Valjent, E., Biever, A., Gangarossa, G., and Puighermanal, E. (2019). Dopamine
1216 signaling in the striatum. In *Advances in Protein Chemistry and Structural Biology*,
1217 (Academic Press), p.
- 1218 Wang, G.-J., Geliebter, A., Volkow, N.D., Telang, F.W., Logan, J., Jayne, M.C.,
1219 Galanti, K., Selig, P.A., Han, H., Zhu, W., et al. (2011). Enhanced striatal dopamine
1220 release during food stimulation in binge eating disorder. *Obesity (Silver Spring)* 19,
1221 1601–1608.
- 1222 Wang, X.-F., Liu, J.-J., Xia, J., Liu, J., Mirabella, V., and Pang, Z.P. (2015).
1223 Endogenous Glucagon-like Peptide-1 Suppresses High-Fat Food Intake by Reducing
1224 Synaptic Drive onto Mesolimbic Dopamine Neurons. *Cell Rep* 12, 726–733.
- 1225 Wei, W., Pham, K., Gammons, J.W., Sutherland, D., Liu, Y., Smith, A., Kaczorowski,
1226 C.C., and O’Connell, K.M.S. (2015). Diet composition, not calorie intake, rapidly
1227 alters intrinsic excitability of hypothalamic AgRP/NPY neurons in mice. *Sci Rep* 5,
1228 16810.
- 1229 Wise, R.A. (2004). Dopamine, learning and motivation. *Nat. Rev. Neurosci.* 5, 483–
1230 494.

1231 **Figure legends**

1232

1233 **Figure 1: Allostatic adaptations of metabolic efficiency to time-locked access**

1234 **to palatable diet. (A)** Experimental design. Control animals (Ctr) or bingeing animals

1235 (Binge) had daily intermittent access to water or a palatable mixture for 1 hour.

1236 Regular chow pellets were provided *ad libitum* throughout the entire experiment.

1237 Pictures show the gut of animals after the last binge session. **(B)** Daily binge

1238 consumption (ml) of palatable mixture during a 14-days protocol. Statistics:

1239 *** $p < 0.001$ Binge vs Control. **(C)** 24 hrs locomotor activity in calorimetric chambers

1240 (average of 3 consecutive days). Red dotted rectangles indicate the locomotor

1241 activity 2 hrs prior and after palatable food access. Statistics: * $p < 0.05$ and ** $p < 0.01$

1242 Binge vs Control. **(C¹)** Cumulative locomotor activity two hours prior and after

1243 palatable food access. Results are expressed as beam breaks (bb). Statistics:

1244 * $p < 0.05$ and *** $p < 0.001$ Binge vs Control. **(D)** Temporal pattern of regular chow food

1245 intake (FI, kcal/h) during 24 hrs (average of 3 consecutive days). Statistics: ** $p < 0.01$

1246 Binge vs Control. **(D¹)** Cumulative chow food intake during the dark period. Statistics:

1247 *** $p < 0.001$ Binge vs Control. **(E)** 24 hrs food intake considering all calories: standard

1248 diet (SD) and palatable food (PF). Statistics: *** $p < 0.001$ Binge(SD) vs Control(SD),

1249 ### $p < 0.001$ Binge(SD+PF) vs Binge(SD). Note: standard diet (SD), palatable food

1250 (FD). **(F)** Animals' body weight throughout the entire experimental procedure. **(G)**

1251 Longitudinal profile of the respiratory energy ratio (RER) from indirect calorimetry

1252 (average of 3 consecutive days) and **(G¹)** averaged RER values 2 hours prior and

1253 after palatable food access. Statistics: ** $p < 0.01$ and *** $p < 0.001$ Binge vs Control. **(H)**

1254 Longitudinal profile of energy expenditure (EE) from indirect calorimetry (average of 3

1255 consecutive days) and **(H¹)** averaged EE values 2 hours prior and after palatable

1256 food access. Statistics: * $p < 0.05$ and ** $p < 0.01$ Binge vs Control. **(I)** Brown adipose

1257 tissue (BAT) temperature during bingeing. Statistics: * $p < 0.05$ and ** $p < 0.01$ Binge vs

1258 Control. **(J)** Real-time core temperature recording during 24 hrs and **(J¹)** averaged

1259 values 2 hours prior and after palatable food access. Statistics: *** $p < 0.001$ Binge vs

1260 Control. **(K)** Matching locomotor activity from core temperature measurements.

1261 Statistics: *** $p < 0.001$ Binge vs Control. For number of mice/group and statistical

1262 details see **Suppl. Table 1**.

1263

1264 **Figure 2: Peripheral signals adapt to time-locked access to palatable diet. (A)**
1265 Plasma triglycerides (TG), **(B)** insulin and **(C)** corticosterone levels in animals
1266 exposed to water (Control), 1h prior (Anticipation) or 1h after (Consumption) access
1267 to palatable diet. Statistics: * $p < 0.05$ and *** $p < 0.001$ Anticipation vs Control, ### $p < 0.01$
1268 Consumption vs Anticipation. **(D)** Blood glucose and **(E)** insulin levels in animals daily
1269 exposed to water (Ctr) or palatable diet (binge) after an oral glucose tolerance test
1270 (OGTT). Statistics: * $p < 0.05$ Binge vs Control only at 30 min post OGTT. **(D¹** and **E¹)**
1271 Glucose and insulin AUC, respectively. For number of mice/group and statistical
1272 details see **Suppl. Table 1**.

1273

1274 **Figure 3: Binge eating induces dopamine-related molecular modifications. A.** 1
1275 hour consumption of water (Ctr) or palatable diet (Anticipation, Binge) during the
1276 paradigm. On day 14, “acute” animals were exposed to palatable diet for the first time
1277 while “anticipation” animals did not receive the food-reward. **(B)** Punches were
1278 extracted from the dorsal striatum (DS) and nucleus accumbens (NAc) for western
1279 blotting analysis. Phosphorylated ERK1/2, ribosomal protein S6 Ser^{235/236} (P-
1280 S6^{S235/236}) and phosphorylated ribosomal protein S6 Ser^{240/244} (P-S6^{S240/244})
1281 expression in the DS and NAc **(C)**. **(D, E)** Protein quantification of phospho-ERK,
1282 S6^{S235/236} and S6^{S240/244} in the DS **(D)** and NAc **(E)**. Statistics: * $p < 0.05$, ** $p < 0.01$ and
1283 *** $p < 0.001$ Binge or Anticipation vs Control. **(F, G)** Immunolabeling and quantification
1284 of phosphorylated rpS6 in the DS (F) and NAc (G) in control and binge animals.
1285 Statistics: *** $p < 0.001$ Binge vs Control. For number of mice/group and statistical
1286 details see **Suppl. Table 1**.

1287

1288 **Figure 4: Binge eating induces dopamine-related modifications in a D1R-**
1289 **dependent manner. (A, B)** Temporal profile of locomotor activity and cumulative
1290 locomotor response (**A¹** and **B¹**) of animals treated with the dopamine-transport
1291 blocker GBR during the anticipatory phase (**A, A¹**) or one hour after intermittent
1292 access to water (Ctr + GBR) or palatable diet (Binge + GBR) (**B, B¹**). Results are
1293 expressed as beam breaks (bb). Statistics: ** $p < 0.01$ Binge+GBR vs Control+GBR.
1294 **(C)** Palatable diet intake after vehicle (Veh+Binge) or D1R antagonist SCH23390
1295 (SCH+Binge) treatment. Statistics: *** $p < 0.001$ SCH+Binge vs Veh+Binge. **(D)**
1296 Palatable diet intake after vehicle (Veh+Binge) or D2R antagonist haloperidol 0.25
1297 mg/kg or 0.5 mg/kg (H^{0.25}+Binge and H^{0.5}+Binge) treatment. Immunolabeling of

1298 phosphorylated rpS6 in the DS (**E**) and NAc (**F**) and their associated quantifications
1299 (**E**¹, **E**², **F**¹, **F**²) in mice pretreated with SCH23390 or vehicle and exposed to time-
1300 locked palatable diet. Statistics: ***p<0.001 Veh+Binge vs Veh+Control, ###p<0.001
1301 SCH+Binge vs Veh+Binge. (**G**) Temporal profile of locomotor activity and cumulative
1302 locomotor response (**G**¹) of animals receiving SCH (SCH+Binge) or vehicle
1303 (Veh+Binge) (red arrow) and access to palatable diet (black arrow). Statistics:
1304 **p<0.01 SCH+Binge vs Veh+Binge. (**H**) Cumulative regular chow diet intake
1305 following SCH23390 (SCH+Binge) or vehicle (Veh+Binge). Statistics: **p<0.01
1306 SCH+Binge vs Veh+Binge. (**I**) Temporal profile of locomotor activity and cumulative
1307 locomotor response (2 hrs and 30 min, **I**¹) induced by the D1R agonist SKF81297
1308 administered 1 hour after access to time-locked water (Ctr+SKF) or palatable diet
1309 (Binge+SKF). Statistics: *p<0.05 and **p<0.01 Binge+SKF vs Control+SKF. For
1310 number of mice/group and statistical details see **Suppl. Table 1**.

1311

1312 **Figure 5: Peripheral endocannabinoids (eCBs) govern binge eating.** (**A**)
1313 Palatable bingeing in animals pretreated with vehicle (Veh), leptin, insulin, GLP1
1314 agonists exendin-4 (Exe4) and liraglutide (Lira), CCK octapeptide sulfated (CCK-8S)
1315 or CB1R inverse agonist AM251. Statistics: ***p<0.001 Exe4-, Lira-, CCK-8S- &
1316 AM251-treated Bingeing mice vs Veh+Binge mice, ###p<0.001 AM251-treated vs
1317 Exe4-, Lira & CCK-8S-treated bingeing mice. (**B**) Dosage of peripheral and
1318 circulating endocannabinoids: anandamide (AEA), diacylglycerol (2-AG),
1319 docosahexanoyl ethanolamide (DHEA) and oleoylethanolamide (OEA) 1 hour before
1320 and 1 hour after palatable bingeing. (**C**) Palatable bingeing in animals pre-treated
1321 with a single i.p. injection of vehicle (Veh), peripheral CB1R antagonist AM6545 (10
1322 mg/kg), and/or monoacylglycerol lipase inhibitor JZL184 (8 mg/kg). Statistics:
1323 ***p<0.001 AM6545, JZL184, AM6545+JZL184 vs Veh-Binge. (**D**) Chronic effect of
1324 JZL184 and AM6545 on palatable bingeing. Statistics: ***p<0.001 AM6545-Binge vs
1325 Veh-Binge, ###p<0.001 JZL184-Binge vs Veh-Binge. (**E, F**) Effects of AM6545 on
1326 core temperature (**E**) and locomotor activity (**F**). Statistics: **p<0.01 AM6545-Binge
1327 vs Veh-Binge. Note: black and red arrows indicate administration of AM6545 and
1328 palatable food access, respectively. (**G**) Longitudinal measurement of fatty acid
1329 oxidation (FAO) following administration of AM6545 during a Binge session and a
1330 NoBinge session. (**G**¹) Averaged FAO from time of injection (11h00) till the end of
1331 light phase (19h00). (**G**²) Ratio of FAO and food intake to discriminate between the

1332 effect of AM6545 and calories intake. Statistics: *** $p < 0.001$ AM6545 vs Veh (in both
1333 Binge and NoBinge sessions). (H) Palatable bingeing after oral gavage of AM6545
1334 (10 mg/kg, p.o.) and associated fatty acids oxidation (I). (J) The scheme indicates
1335 gut-originated afferent paths that were virally targeted to perform single-cell
1336 transcriptomic analysis (Bai et al., 2019). (K) Enrichment of different vagal markers
1337 (*SLC17a6*, *Scn10a*, *Htr3a*, *Cartpt*, *Grin1*, *Phox2b*) and comparison with *Cnr1* and
1338 *Cnr2* in sensory vagal neurons labeled from microinjections in the stomach, proximal
1339 and middle intestines. For number of mice/group and statistical details see **Suppl.**
1340 **Table 1.**

1341

1342 **Figure 6: The gut-brain vagal axis is required for eCBs-mediated effects. (A, B)**
1343 cFos immunolabeling in the area postrema (AP), the nucleus tractus solitarius (NTS),
1344 the lateral parabrachial nucleus (IPBN) and medial parabrachial nucleus (mPBN) in
1345 sham and vagotomized animals treated with the peripheral CB1R antagonist AM6545
1346 (10 mg/kg). (A¹) Scheme indicates the central vagus→NTS→PBN→target regions
1347 path in VGX mice. (A²) Quantification of cFos-positive neurons in the AP, NTS and
1348 IPBN in sham and VGX mice injected with AM6545. Statistics: *** $p < 0.001$
1349 VGX+AM6545 vs Sham+AM6545. (B) Palatable bingeing in sham and vagotomized
1350 (VGX) animals pre-treated with AM6545 (A) or vehicle (V), and associated
1351 measurements of fatty acid oxidation (C, C¹ and D, D¹). Statistics: *** $p < 0.001$
1352 Sham+AM6545 vs Sham+Veh. (E) cFos immunolabeling of paraventricular nucleus
1353 of the hypothalamus (PVN) and dorsomedial nucleus of the hypothalamus (DMH) in
1354 sham or VGX animals treated with vehicle or AM5646 and associated counting (E¹).
1355 Statistics: *** $p < 0.001$ Sham+AM6545 vs Veh, #### $p < 0.001$ VGX+AM6545 vs
1356 Sham+AM6545. For number of mice/group and statistical details see **Suppl. Table**
1357 **1.**

1358

1359 **Figure 7: Peripheral CB1R signaling routed by the vagus nerve controls VTA**
1360 **DA-neurons activity. (A, A¹)** Effect of AM6545 or Veh on GBR-induced locomotor
1361 activity (beam breaks, bb). Statistics: ** $p < 0.01$ AM6545+GBR vs Veh+GBR. (B, B¹)
1362 Effect of AM6545 on GBR-triggered cFos in the striatum. Statistics: *** $p < 0.001$
1363 AM6545+GBR vs Veh+GBR. (C) Amphetamine (Amph)-induced locomotor activity
1364 and (C¹) cumulative locomotor response (C1) in mice pretreated with vehicle
1365 (Veh+Amph) or AM6545 (AM6545+Amph). GBR-induced locomotor activity (D),

1366 cumulative locomotor response (**D**¹) in VGX mice pretreated with vehicle
1367 (VGX/Veh+GBR) or AM6545 (VGX/AM6545+GBR). GBR-induced locomotor activity
1368 (**E**) and cumulative locomotor response (**E**¹) in mice pretreated with oral gavage of
1369 vehicle (Veh (po)+GBR) or AM6545 (AM6545 (po)+GBR). (**F**) Expression of
1370 GCaMP6f in VTA dopamine neurons of virally injected *Drd2-Cre* mice. Please, note
1371 colocalization with TH and GCaMP6f-positive terminals in the striatum and NAc. (**G**)
1372 Behavioral paradigms used to trigger the activity of VTA dopamine neurons:
1373 exposure to a new environment (new cage) and tail suspension. (**H**) Temporal
1374 dynamics of DA-neurons activity during the exposure to a new environment (new
1375 cage). Statistics: **p<0.01 AM6545 vs Veh. (**I**) Temporal dynamics of DA-neurons
1376 activity during the tail suspension test. Statistics: **p<0.01 AM6545 vs Veh. For
1377 number of mice/group and statistical details see **Suppl. Table 1**.

1378

1379 **Supplemental Figure 1: Adaptations to time-locked palatable feeding.** (**A**) Binge
1380 consumption and (**B**) time to first lick during the last BE session of milkshake
1381 (lipids+sucrose), sucralose (2 mM) and saccharin (0.1% w/v). Statistics: ***p<0.001
1382 Sucralose or Saccharin vs Milkshake (Lipids/Sucrose). Body composition [fat mass,
1383 (**C**) and lean mass (**D**)] of control and bingeing mice. (**E**) Longitudinal profile of the
1384 fatty acids oxidation (FAO) from indirect calorimetry measurements (average of 3
1385 consecutive days). For number of mice/group and statistical details see **Suppl. Table**
1386 **1**.

1387

1388 **Supplemental Figure 2: Peripheral CB1R and vagal afferents.** (**A**) Longitudinal
1389 measurement of fatty acid oxidation (FAO) following oral administration of AM6545
1390 (10 mg/kg). Note no modification in FAO. (**B, C**) Expression of *Cnr1* in sensory vagal
1391 neurons labeled from microinjections in the distal and large intestines. For number of
1392 mice/group and statistical details see **Suppl. Table 1**.

1393

1394 **Supplemental Figure 3: Homeostatic adaptations in sham and VGX mice during**
1395 **time-locked palatable feeding.** (**A**) 24 hours measurement of chow food intake in
1396 sham and VGX bingeing mice. Statistics: ***p<0.001 VGX+Binge vs Sham+Binge.
1397 (**B**) Body weight of both experimental groups. (**C-E**) Respiratory exchange ratio
1398 (RER), fatty acids oxidation (FAO) and energy expenditure (EE) in sham and VGX

1399 mice during a binge session. Statistics: * $p < 0.05$, ** $p < 0.01$ VGX+Binge vs
1400 Sham+Binge. For number of mice/group and statistical details see **Suppl. Table 1**.

1401

1402 **Supplemental Figure 4: *In vivo* recoding of Ca^{2+} transients in VTA dopamine**
1403 **neurons of *Drd2-Cre* mice. (A)** Ca^{2+} transients evoked following presentation of a
1404 high-fat high-sugar (HFHS) pellet (positive and reinforcing stimulus). Statistics:
1405 *** $p < 0.001$ HFHS_{after} vs HFHS_{before}. **(B)** Ca^{2+} transients evoked following scruff
1406 restraint (negative stimulus). Note: artefact signals while restraining the mouse were
1407 not included in the analysis. Statistics: *** $p < 0.001$ Scruff_{after} vs Scruff_{before}. For
1408 number of mice/group and statistical details see **Suppl. Table 1**.

Graphical Abstract Berland et al.,

bioRxiv preprint doi: <https://doi.org/10.1101/2020.11.14.382291>; this version posted November 16, 2020. The copyright holder for this preprint (which was not certified by peer review) is the author/funder, who has granted bioRxiv a license to display the preprint in perpetuity. It is made available under a [CC-BY-NC-ND 4.0 International license](#).

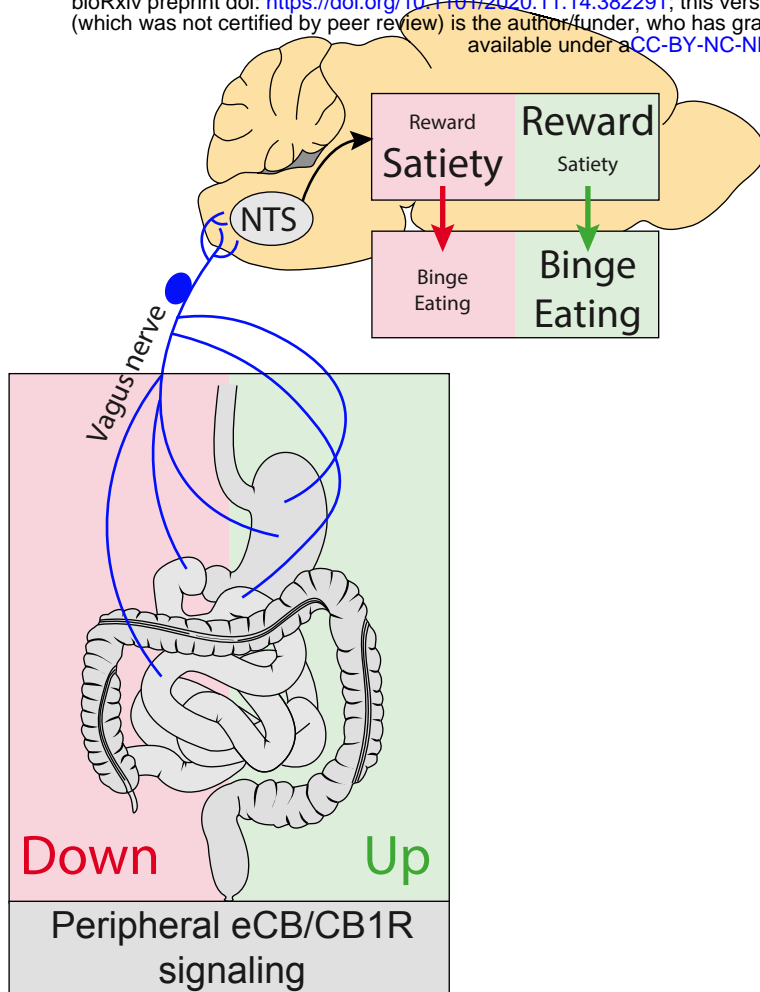


Figure 1 Berland et al.,

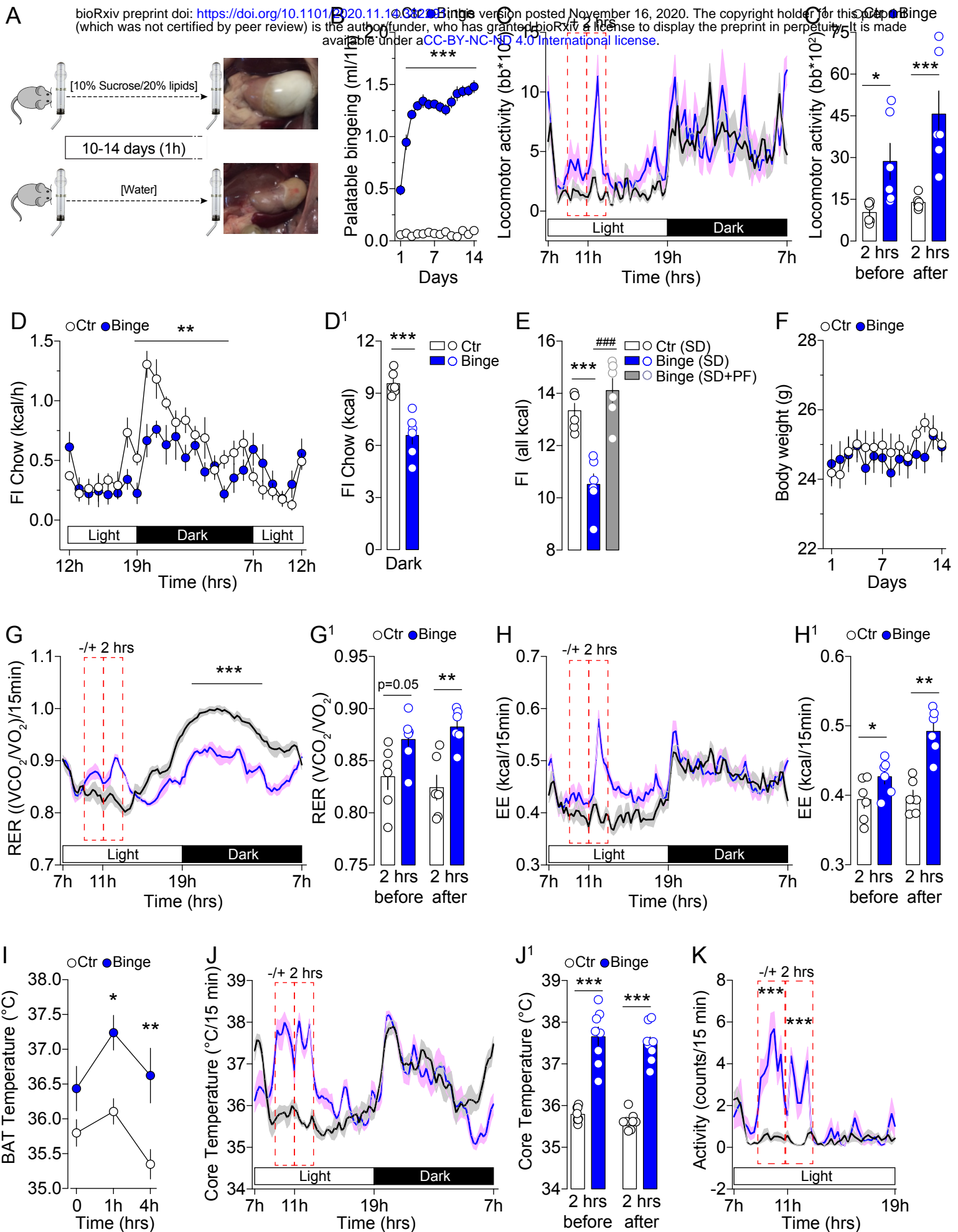


Figure 2 Berland et al.,

bioRxiv preprint doi: <https://doi.org/10.1101/2020.11.14.382291>; this version posted November 16, 2020. The copyright holder for this preprint (which was not certified by peer review) is the author/funder, who has granted bioRxiv a license to display the preprint in perpetuity. It is made available under a [CC-BY-NC-ND 4.0 International license](https://creativecommons.org/licenses/by-nc-nd/4.0/).

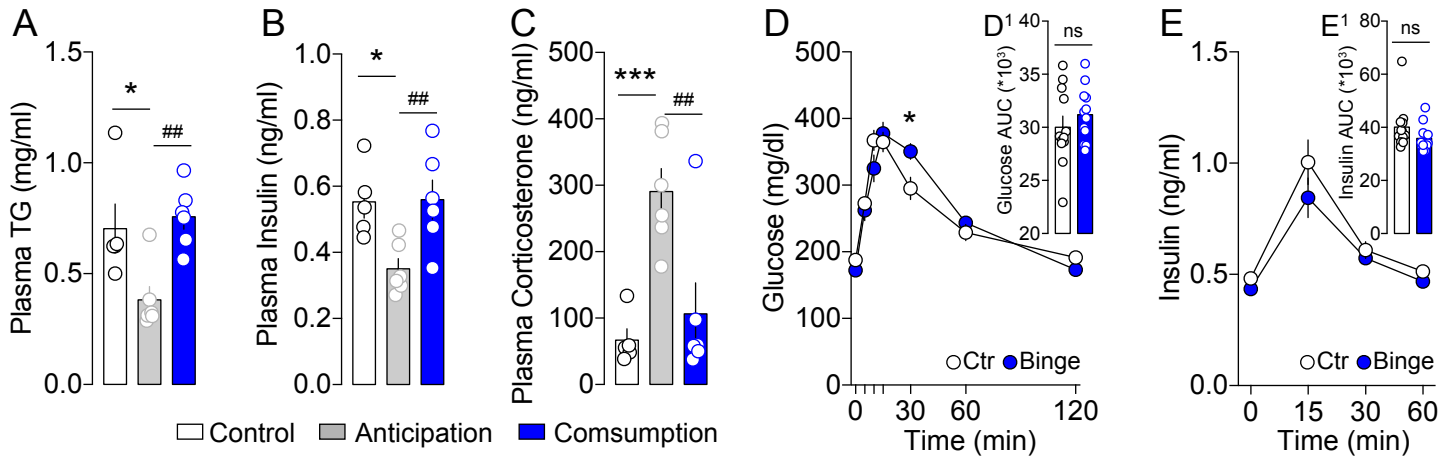


Figure 3 Berland et al.,

bioRxiv preprint doi: <https://doi.org/10.1101/2020.11.14.382291>; this version posted November 16, 2020. The copyright holder for this preprint (which was not certified by peer review) is the author/funder, who has granted bioRxiv a license to display the preprint in perpetuity. It is made available under a [CC-BY-NC-ND 4.0 International license](#).

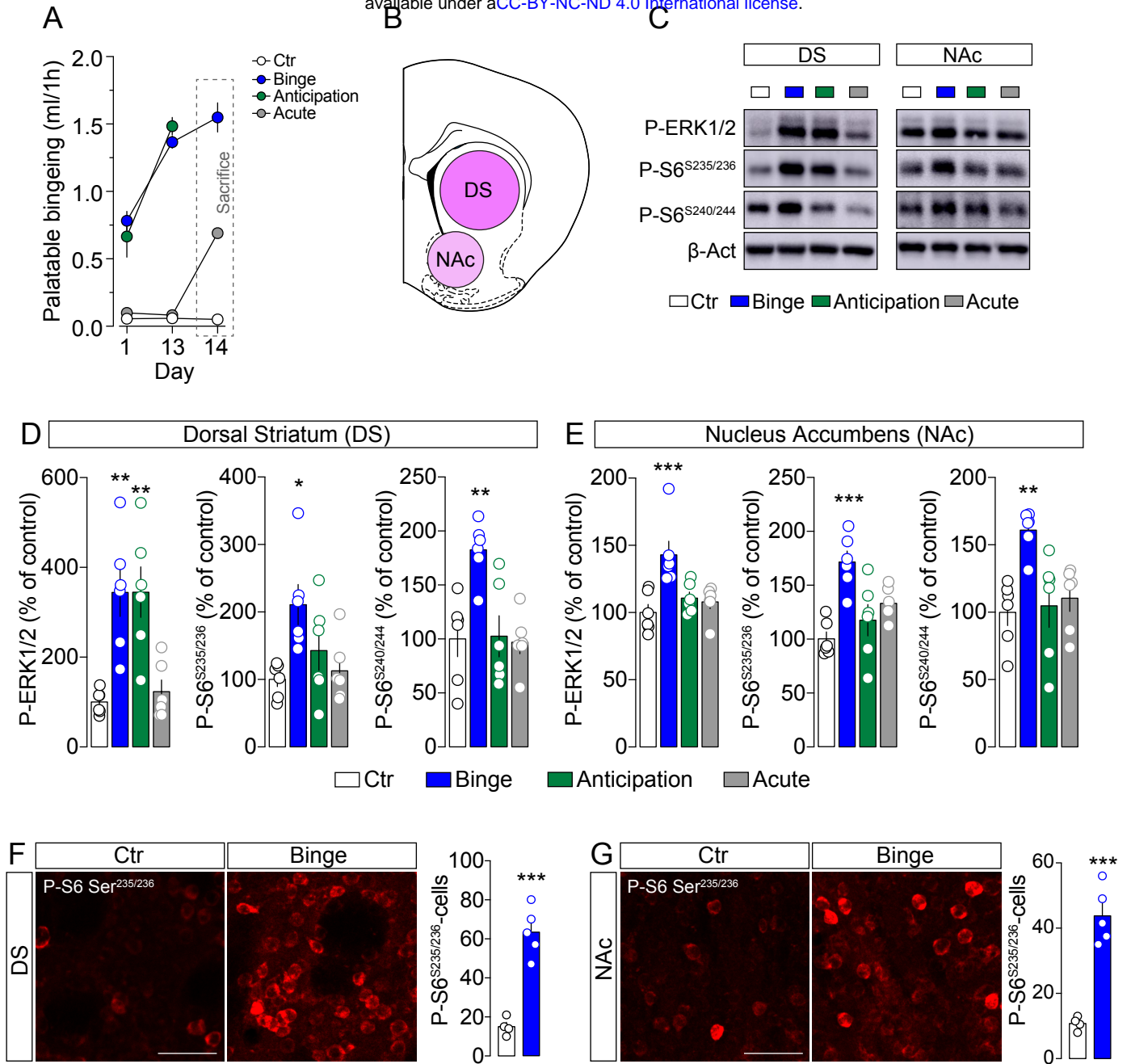


Figure 4 Berland et al.,

bioRxiv preprint doi: <https://doi.org/10.1101/2020.11.14.382291>; this version posted November 16, 2020. The copyright holder for this preprint (which was not certified by peer review) is the author/funder, who has granted bioRxiv a license to display the preprint in perpetuity. It is made available under aCC-BY-NC-ND 4.0 International license.

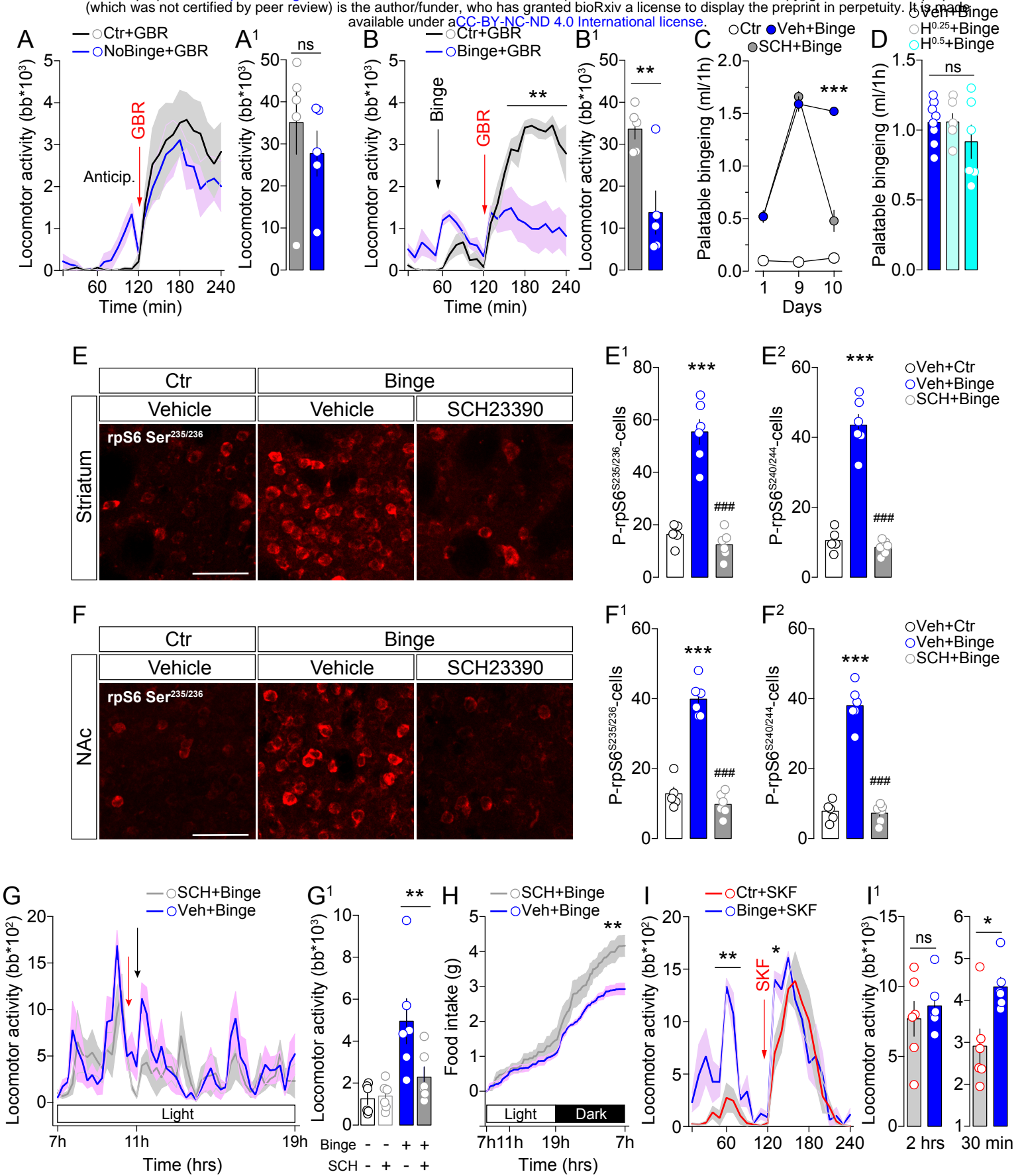


Figure 5 Berland et al.,

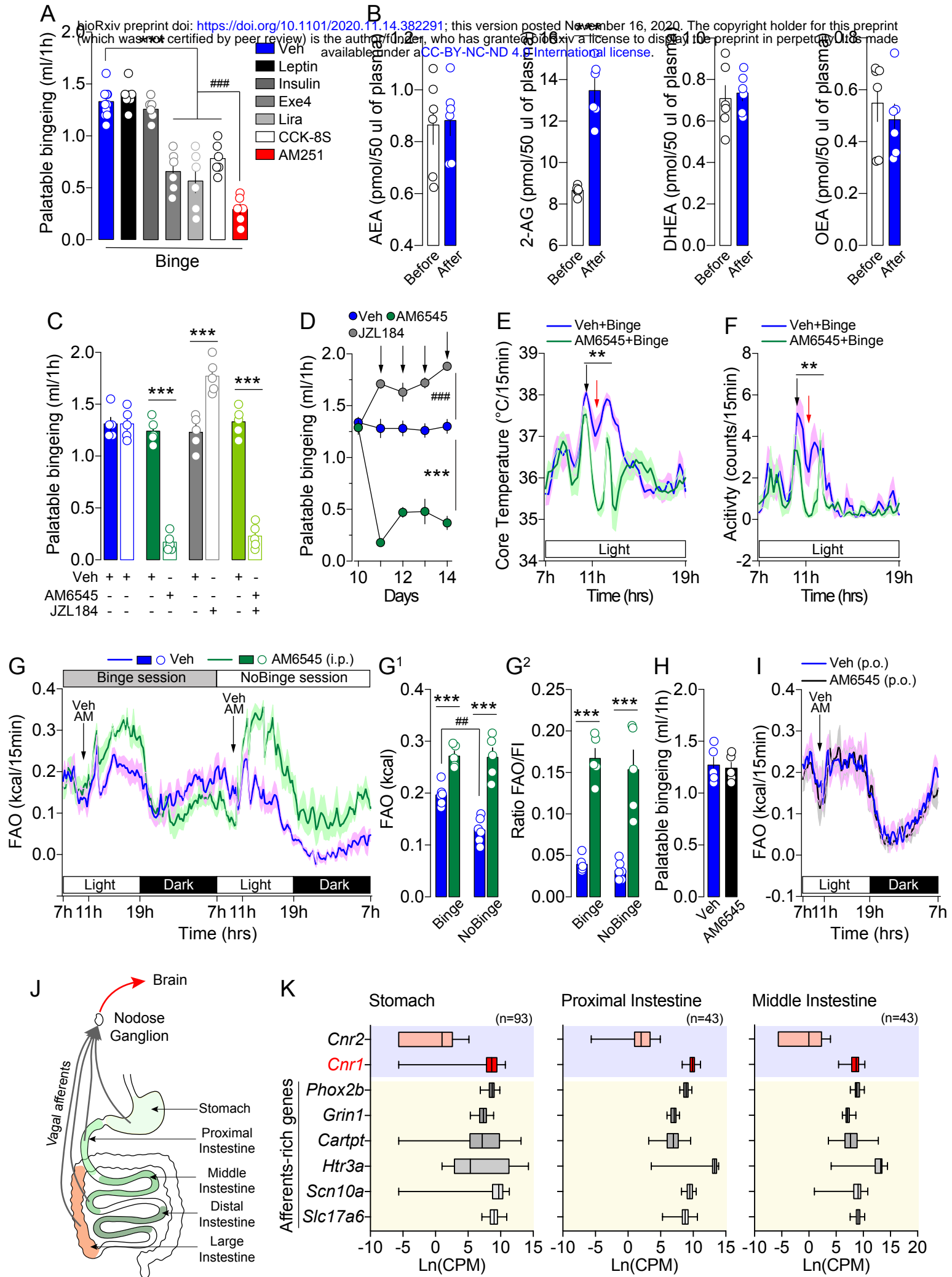


Figure 6 Berland et al.,

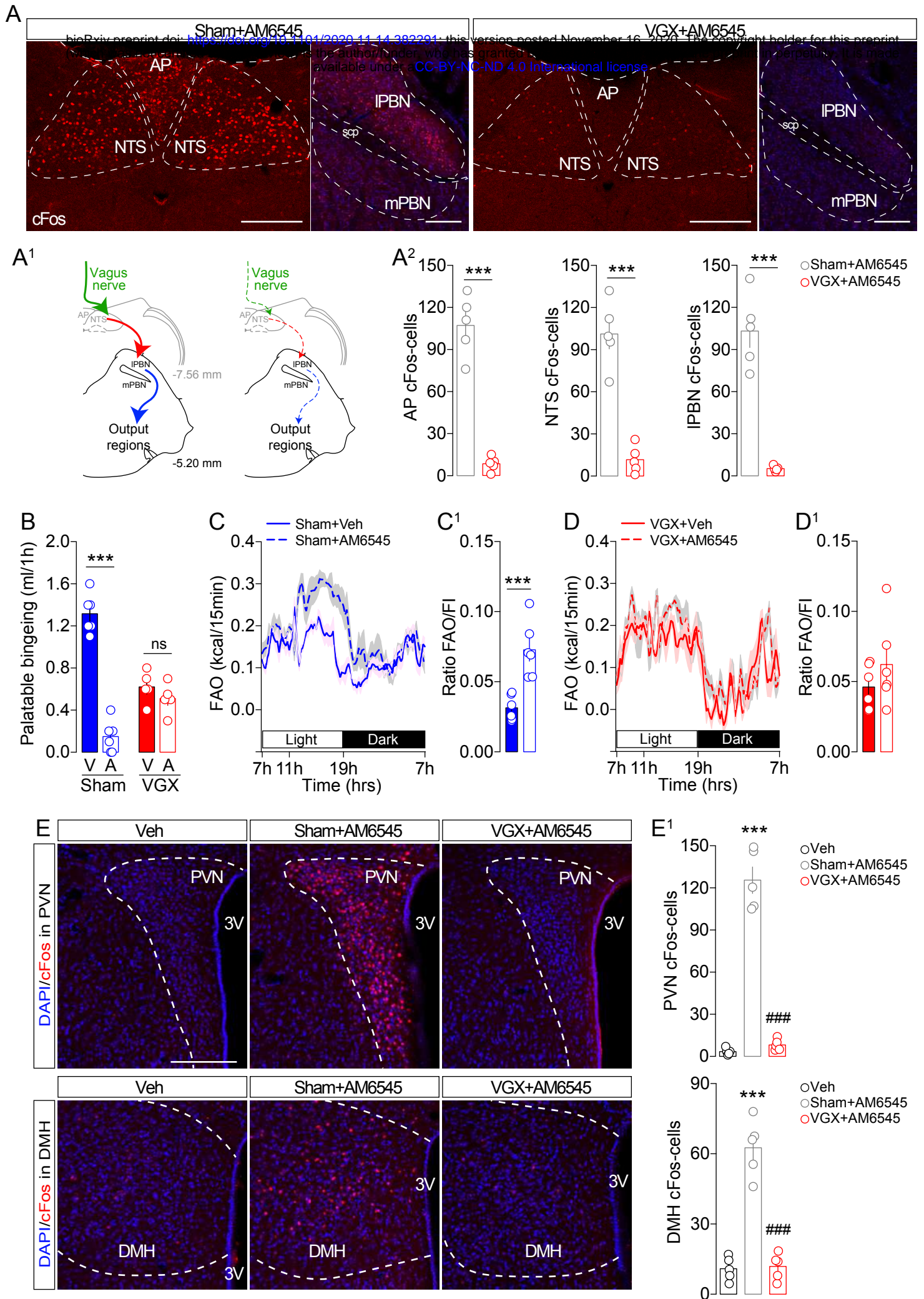
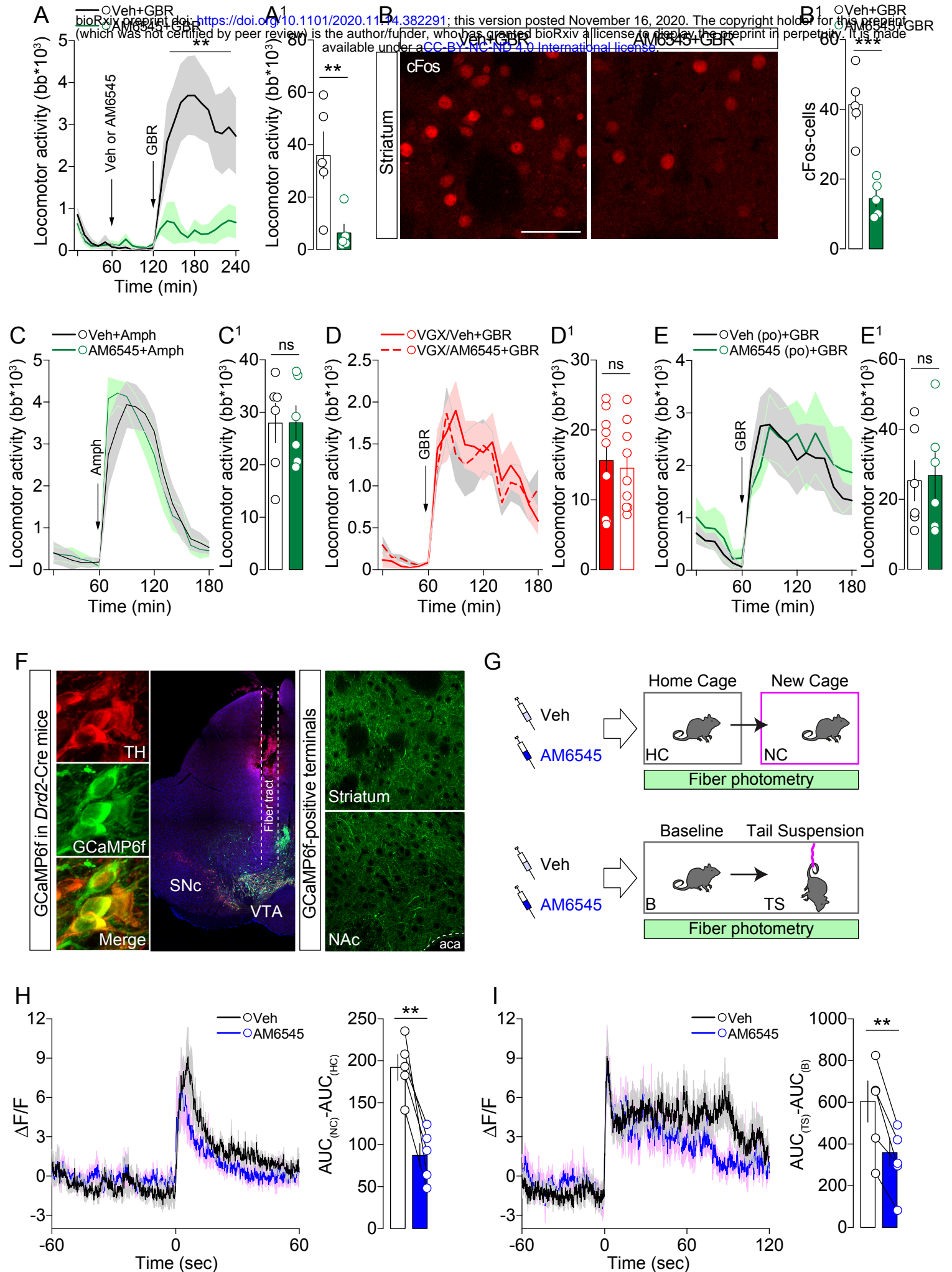
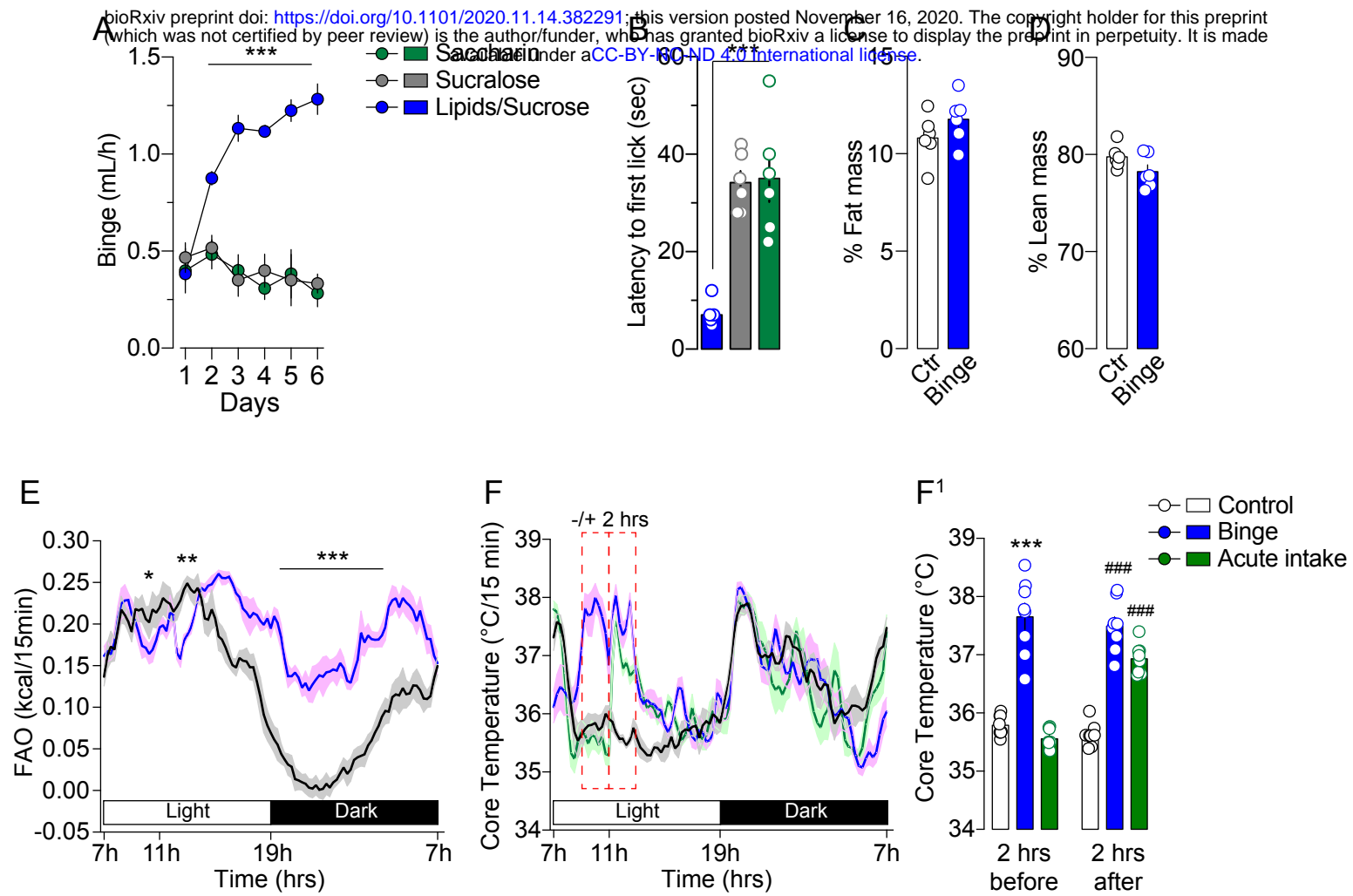


Figure 7 Berland et al.,



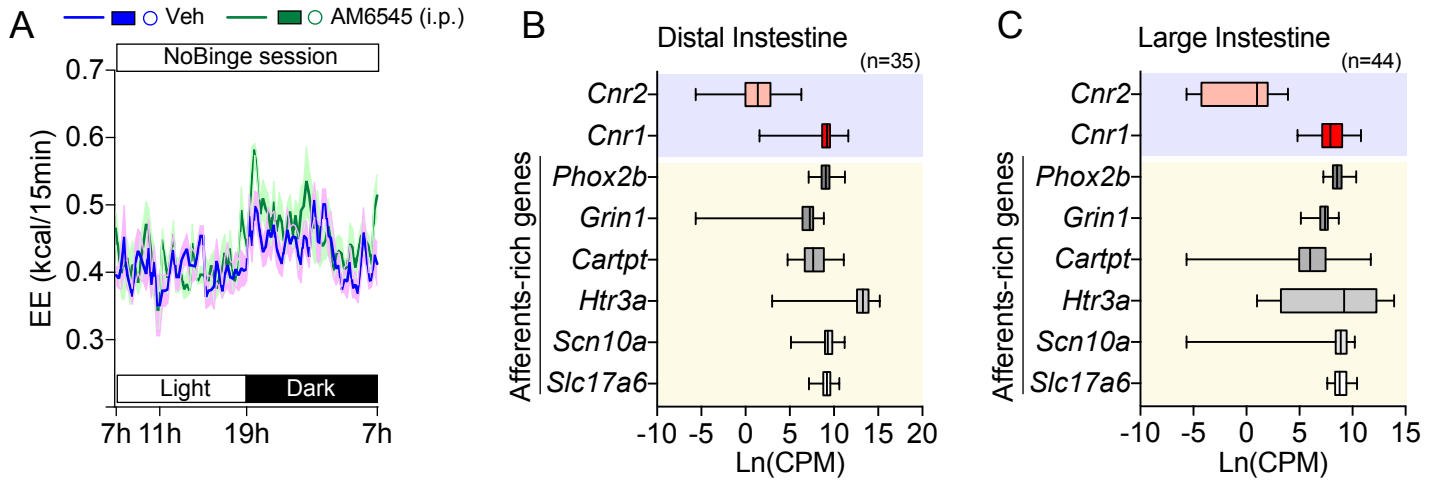
Suppl. Figure 1 Berland et al.,

bioRxiv preprint doi: <https://doi.org/10.1101/2020.11.14.382291>; this version posted November 16, 2020. The copyright holder for this preprint (which was not certified by peer review) is the author/funder, who has granted bioRxiv a license to display the preprint in perpetuity. It is made available under aCC-BY-ND 4.0 International license.



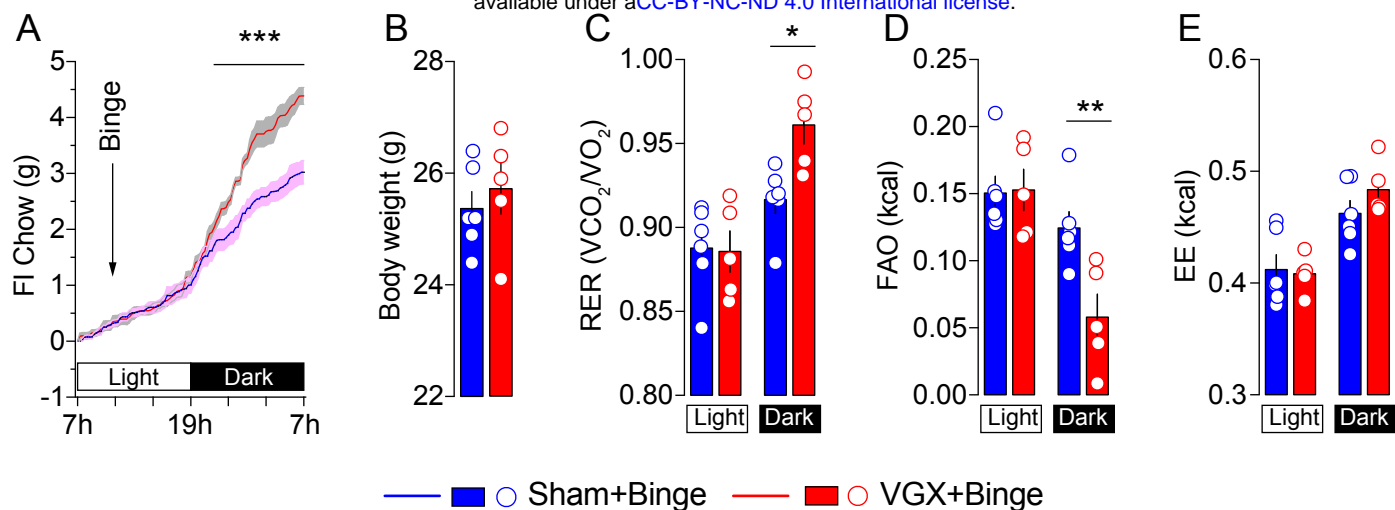
Suppl. Figure 2 Berland et al.,

bioRxiv preprint doi: <https://doi.org/10.1101/2020.11.14.382291>; this version posted November 16, 2020. The copyright holder for this preprint (which was not certified by peer review) is the author/funder, who has granted bioRxiv a license to display the preprint in perpetuity. It is made available under a [CC-BY-NC-ND 4.0 International license](#).



Suppl. Figure 3 Berland et al.,

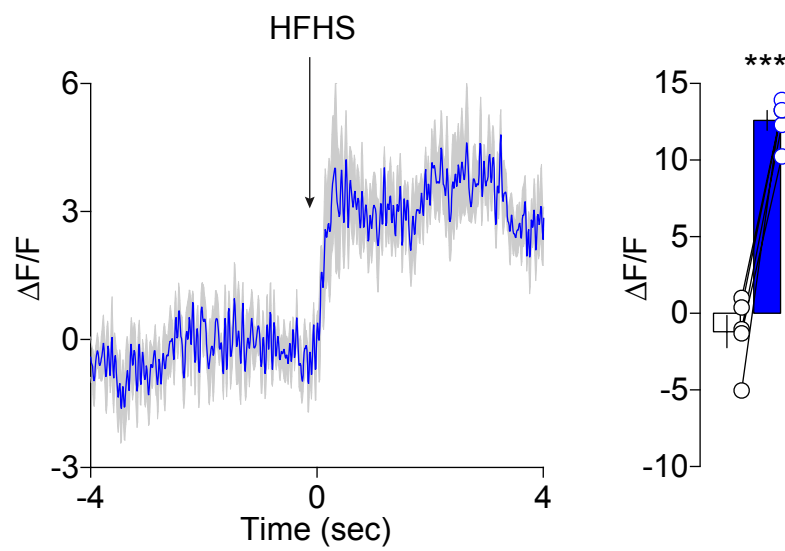
bioRxiv preprint doi: <https://doi.org/10.1101/2020.11.14.382291>; this version posted November 16, 2020. The copyright holder for this preprint (which was not certified by peer review) is the author/funder, who has granted bioRxiv a license to display the preprint in perpetuity. It is made available under a [CC-BY-NC-ND 4.0 International license](#).



Suppl. Figure 3 Berland et al.,

bioRxiv preprint doi: <https://doi.org/10.1101/2020.11.14.382291>; this version posted November 16, 2020. The copyright holder for this preprint (which was not certified by peer review) is the author/funder, who has granted bioRxiv a license to display the preprint in perpetuity. It is made available under aCC-BY-NC-ND 4.0 International license.

A Positive valence: HFHS relief



B Negative valence: Scruff restraint

